Paleoproterozoic S-type granites in the Helanshan Complex, Khondalite Belt, North China Craton: Implications for rapid sediment recycling during slab break-off

Wei Dan[a, b*], Xian-Hua Li[b], Qiang Wang[a*], Xuan-Ce Wang[c], Yu Liu[b], Derek A. Wyman[d]

[a] State Key Laboratory of Isotope Geochemistry, Guangzhou Institute of Geochemistry, Chinese Academy of Sciences, Guangzhou, Guangdong 510640, China

[b] State Key Laboratory of Lithospheric Evolution, Institute of Geology and Geophysics, Chinese Academy of Sciences, Beijing 100029, China

[c] ARC Center of Excellence for Core to Crust Fluid Systems (CCFS) and The Institute for Geoscience Research, Department of Applied Geology, Curtin University of Technology, Perth, WA 6845, Australia

[d] School of Geosciences, The University of Sydney, NSW 2006, Australia

Corresponding authors:
Dr. Wei Dan
State Key Laboratory of Isotope Geochemistry, Guangzhou Institute of Geochemistry, Chinese Academy of Sciences, Guangzhou, Guangdong 510640, China
E-mail address: danwei@gig.ac.cn
Tel: +86 20 85292986; fax: +86 20 85290130

Prof. Qiang Wang
State Key Laboratory of Isotope Geochemistry, Guangzhou Institute of Geochemistry, Chinese Academy of Sciences, Guangzhou, Guangdong 510640, China
E-mail address: wqiang@gig.ac.cn
Tel: +86 20 85290277; fax: +86 20 85290130

Abstract

S-type granites, typically derived from the rapid recycling of sedimentary rocks, are sometimes accompanied by contemporary mafic magmatism and granulite metamorphism. However, the geodynamic context for such rock suites is often highly disputed, with various model proposed, including back-arc basin opening, lithospheric delamination, mantle plume and continental rifting. The Paleoproterozoic Khondalite Belt in the North China Craton provides an example of synchronous mafic and felsic magmatism that was accompanied by granulite-facies metamorphic events for which the tectonic affinities of these rocks remains unclear. This study integrates *in situ* zircon Hf–O isotope analyses, whole-rock geochemistry and Nd isotope results for the earliest two-mica granites (ca. 1.95 Ga) in order to provide constraints on the above issues. The granites are strongly peraluminous (A/CNK value >1.1), and characterized by high zircon $\delta^{18}O$ values of 7.3 to 10.6‰, corresponding to calculated magmatic $\delta^{18}O$ values of 9.1 to 12.3‰, similar to those of typical S-type granites. They have relatively high and homogeneous $\varepsilon_{Nd}(t)$ values of -1.1 to +0.9 and highly variable zircon $\varepsilon_{Hf}(t)$ values ranging from -1.0 to +8.3. *In situ* zircon Hf-O isotopic compositions indicate that the S-type granites may contain some mantle or juvenile crustal components in addition to a sediment component. Based on the new results and published data, a slab break-off model is proposed to explain the rapid recycling of sedimentary precursors and the generation of the ca. 1.95 Ga S-type granites.

Keywords: S-type granite; slab break-off; zircon Hf-O isotopes; Paleoproterozoic; North China Craton

1. Introduction

Accretionary and collisional orogens are important sites for the partial melting of recycled sedimentary rocks to form S-type granites (e.g., Sylvester, 1998; Barbarin, 1999; Collins and Richards, 2008; Kemp et al., 2009). The time interval between the deposition of sedimentary rocks and formation of magmatic rocks can be less than 50 m.y. (e.g., Kemp et al., 2007; Zheng et al., 2008). Several mechanisms have been proposed to explain the rapid formation of S-type granites. For subduction systems or accretionary orogens, the rapid formation of S-type granites and related rocks has been accounted for by models of back-arc basin opening (Cenozoic Hidaka metamorphic belt, Japan; Kemp et al., 2007) and lithospheric delamination (Ordovician Lachlan Fold Belt, Australia; Foster and Goscombe, 2013) or by models that combine both features (Collins and Richards, 2008). The rapid formation of S-type granites in collisional orogenic belts, however, has commonly been attributed to mantle plumes (Jiangnan Orogen, South China Block, Li et al., 2003) or continental rifting (Jiangnan Orogen, Zheng et al., 2008). In some cases, coeval granulites and mafic magmatism accompanied sediment recycling, as in the Hidaka metamorphic belt, Japan (accretionary orogen, Kemp et al., 2007) and the Silurian Tongbai Orogen, Central China (collisional orogen, Wang et al., 2011a). Such examples of coeval mafic magmatism, felsic magmatism and granulite metamorphism provide multiple constraints on contemporary geodynamics, which can help to resolve the origin of S-type granites.

The Khondalite Belt in the North China Craton is characterized by widely distributed granulite facies metasedimentary rocks, along with dolerite dykes, S-type granites and minor exposures of ultra-high temperature (UHT) rocks (e.g., Lu et al., 1992, 1996; Guo et al., 2006; Santosh et al., 2007a, 2007b; Liu et al., 2012a; Zhang et al., 2012a; Zhao, 2014). Recent high-precision geochronological data have revealed magmatic episodes at ca. 2.56-2.50 Ga, 2.45-2.37 Ga, 2.30-2.00 Ga, 1.97-1.90 Ga and 1.85-1.82 Ga, and metamorphic overprints at ca. 1.95-1.90 Ga and 1.87-1.82 Ga (e.g., Jian et al., 2005; Xia et al., 2006a, b, 2008, 2009; Wan et al., 2006, 2009, 2013a; Yin et al., 2009, 2011; Zhao et al., 2010; Li et al., 2011a; Dan et al., 2012; Ma et al., 2012; Dong et al., 2013, 2014; Liu et al., 2013, 2014; Jiao et al., 2013). The ca. 1.95-1.90 Ga metamorphic event is commonly interpreted to have resulted from collisional orogeny to form the Khondalite Belt collisional orogen (e.g., Zhao et al., 2005, 2010; Yin et al., 2009, 2011, 2014; Zhao and Zhai, 2013). However, numerous ca. 1.97-1.95 Ga magmatic rocks have recently been discovered, including gabbro, carbonatite, gabbronorite, charnockite and S-type granite (Wan et al., 2008, 2013a; Geng et al., 2009; Song et al., 2010; Peng et al., 2010; Dan et al., 2012; Ma et al., 2012; Liu et al., 2013). Accordingly, a revised model is required to account for the formation of these magmatic rocks and the associated metamorphism. In this contribution, we report an integrated study of *in situ* zircon Hf–O isotopes as well as whole-rock geochemistry and Nd isotopes for the earliest S-type granites (ca. 1.95 Ga) (Dan et al., 2012). These new results, combined with available published data, are used to constrain the tectonic setting of the ca. 1.97-1.90 Ga magmatism and the rapidly recycled sedimentary

rocks.

2. Geological background

The North China Craton (NCC) has been divided into four small Archean-Paleoproterozoic continental blocks (i.e., the Longgang, Langrim, Yinshan and Ordos blocks) and three Paleoproterozoic tectonic belts, named the Khondalite Belt, Trans-North China Orogen and Jiao-Liao-Ji Belt (Fig. 1), of which the Khondalite Belt formed by amalgamation of the Yinshan and Ordos blocks to form the Western Block at ~1.95 Ga (Zhao et al., 2005; Yin et al., 2009, 2011), whereas the Jiao-Liao-Ji Belt formed by amalgamation of the Longgang and Langrim blocks to form the Eastern Block at ~1.90 Ga (Li et al., 2004a, 2005a, 2006, 2011b, 2012; Li and Zhao, 2007; Luo et al., 2004, 2008; Zhou et al., 2008; Tam et al., 2011, 2012a,b,c). Finally, the NCC formed by amalgamation of the Eastern and Western blocks along the Trans-North China Orogen (TNCO) at ca. 1.85 Ga (e.g., Guo et al., 2005; Kröner et al., 2005; Zhang et al., 2007, 2009, 2012b; Zhao et al., 2001, 2005, 2010; Lu et al., 2008; Li et al., 2010a; Wang et al., 2010a; Liu et al., 2012b, c, d), though some alternative models have also been proposed for the formation and evolution of the craton (e.g., Kusky and Li, 2003; Kusky et al., 2007; Trap et al., 2007; Wang et al., 2010b), and a detailed overview of these models was given by Zhao and Cawood (2012).

The Khondalite Belt extends northwesterly over 1000 km, consisting of, from

east to west, the Jining, Daqingshan-Ulashan, Qianlishan and Helanshan complexes (Fig. 1). Granulite facies metasedimentary rocks and S-type granites dominate the belt (e.g., Lu et al., 1996). The supracrustal metasedimentary sequences consist of graphite-garnet-sillimanite gneiss, garnet quartzite, felsic paragneiss, calc-silicate rock and marble, referred as the "Khondalite series" in the Chinese literature (Lu et al., 1992, 1996), whose protoliths are traditionally considered to have been deposited on a stable continental margin (Condie et al., 1992; Lu et al., 1992, 1996) and underwent three stages of metamorphism and deformation (Zhao et al., 1999). Recently, based on U-Pb isotopic detrital zircon dating results, Dan et al. (2012) proposed that the protoliths of the Khondalites were sourced mainly from ca. 2.18-2.00 Ga magmatic arcs, deposited on an active continental margin between ca. 2.00 Ga and 1.95 Ga, and then subsequently metamorphosed at ca. 1.95-1.85 Ga (Xia et al., 2006a, b; Wan et al., 2006, 2009; Yin et al., 2009, 2011; Zhao et al., 2010; Guo et al., 2012; Santosh et al., 2013). The age of ca. 1.95 Ga is interpreted to reflect the timing of regional metamorphism linked to the collision and amalgamation of the Yinshan and Ordos blocks (e.g., Yin et al., 2009, 2011, 2014; Zhao et al., 2010; Guo et al., 2012; Santosh et al., 2013). Ultrahigh-temperature (UHT) assemblages have been recognized at several localities in recent years, mainly situated in the eastern Daqingshan-Ulashan and central Jining terranes (e.g., Guo et al., 2006; Santosh et al., 2007a, b; Liu et al., 2010, 2012a; Guo et al., 2012; Zhang et al., 2012a).

The Helanshan Complex is located in the westernmost part of the Khondalite Belt

(Fig. 1) and consists mainly of Khondalite metasedimentary rocks and garnet-bearing S-type granites (Fig. 2). The metasedimentary rocks initially underwent high-grade metamorphism at ca. 1.95 Ga during collision of the Yinshan and Ordos blocks. A second high-grade event at ca. 1.87 Ga was synchronous with the formation of post-orogenic S-type granites (Yin et al., 2011), which have been attributed to anatectic melting of the metasedimentary units (e.g., Hu, 1994; Yin et al., 2011). The known minor granulite occurrences include both high-pressure and high-temperature/low pressure types (Zhou and Geng, 2009; Zhou et al., 2010). Dolerite dykes intruding the Khondalite units have been dated at ca. 1.96 Ga (recalculated from Song et al., 2010). New geochemical analyses were undertaken on the 1947 ± 6 Ma porphyritic K-feldspar granites and 1956 ± 19 Ma two-mica granites, both of which were dated in our previous study (Dan et al., 2012). The porphyritic K-feldspar granite occurs as a dyke, about 15 m wide, that intruded into the metasedimentary rocks (Fig. 3a), and the two-mica granite occurs as a pluton with an outcrop area of 90 km^2. Neither granite exhibits a deformational fabric. The granites have similar mineral assemblages, consisting of K-feldspar (20−50 vol.%) + plagioclase (10−35 vol.%) + quartz (20−40 vol.%) + biotite (3−8 vol.%) + muscovite (1−3 vol.%) (Fig. 3), and trace amounts of magnetite, apatite and zircon.

3. Analytical procedures

3.1. Major and trace elements

Ten rock samples powdered to ~200-mesh size were used for chemical analyses. Major element oxides were analyzed on fused glass beads using a Rigaku RIX 2000 X-ray fluorescence spectrometer at the State Key Laboratory of Isotope Geochemistry, the Guangzhou Institute of Geochemistry, Chinese Academy of Sciences (SKLaBIG-GIG-CAS). Calibration lines used in quantification were produced by bivariate regression of data from 36 reference materials encompassing a wide range of silicate compositions (Li et al., 2005b). Analytical uncertainties are between 1% and 5%. Trace elements were analyzed using an Agilent 7500a ICP-MS at GIG-CAS. Analytical procedures were similar to those described by Li et al. (2000). A set of USGS and Chinese national rock standards, including BHVO-2, GSR-1, GSR-2, GSR-3, AGV-2, W-2 and SARM-4 were chosen for calibration. Analytical precision typically is better than 5%. Geochemical results are listed in Table 1.

3.2. Nd isotopic compositions

Nd isotopic compositions were determined using a Micromass Isoprobe multi-collector ICP-MS at SKLaBIG-GIG-CAS, and analytical procedures described by Li et al. (2004b). Sr and Nd were separated using cation columns, and Nd fractions were further separated by HDEHP-coated Kef columns. The measured $^{143}Nd/^{144}Nd$ ratio of the JNdi-1 standard were 0.512093 ± 11 (n = 11, 2σ). All measured Nd isotope ratios were normalized to $^{146}Nd/^{144}Nd = 0.7219$. The Nd isotope results are listed in Table 2.

185 *3.3. Zircon oxygen isotopes*

186 Zircon oxygen isotopes were measured using the same Cameca IMS-1280 SIMS
187 at IGG-CAS. The detailed analytical procedures were similar to those described by Li
188 et al. (2010b). The measured oxygen isotopic data were corrected for instrumental
189 mass fractionation (IMF) using the Penglai zircon standard ($\delta^{18}O_{VSMOW}$ = 5.3‰) (Li
190 et al., 2010c). The internal precision of a single analysis generally was better than
191 0.2‰ (1σ standard error) for the $^{18}O/^{16}O$ ratio. The external precision, measured by
192 the reproducibility of repeated analyses of Penglai standard, is 0.38‰ (2SD, n = 16).
193 Five measurements of the 91500 zircon standard during the course of this study
194 yielded a weighted mean of $\delta^{18}O$ = 10.2 ± 0.5‰ (2SD), which is consistent within
195 errors with the reported value of 9.9 ± 0.3‰ (Wiedenbeck et al., 2004). Zircon
196 oxygen isotopic data are listed in Table 3.

197

198 *3.4. Zircon Lu–Hf isotopes*

199 *In situ* zircon Lu–Hf isotopic analyses were carried out on a Neptune
200 multi-collector ICP-MS equipped with a Geolas-193 laser-ablation system at
201 IGG-CAS. Lu–Hf isotopic analyses were conducted on the same zircon grains that
202 were previously analyzed for U–Pb and O isotopes, with ablation pits of 60 μm or 44
203 μm in diameter, ablation time of 26 seconds, repetition rate of 8 Hz, and laser beam
204 energy density of 10 J/cm^2. Detailed analytical procedures were similar to those
205 described by Wu et al. (2006). Measured $^{176}Hf/^{177}Hf$ ratios were normalized to

$^{179}Hf/^{177}Hf$ = 0.7325. Further external adjustment was not applied for the unknowns because our determined $^{176}Hf/^{177}Hf$ ratios for zircon standards 91500 (0.282309 ± 0.000004) and GJ-1 (0.282000 ± 0.000008) were in good agreement within errors with the reported values (Griffin et al., 2006; Wu et al., 2006). Zircon Hf isotopic data are listed in Table 3.

4. Results

4.1. Whole-rock major and trace element compositions

The porphyritic K-feldspar granites and two-mica granites from the Helanshan Complex plot in or adjacent to the granite field on a SiO_2 versus K_2O+Na_2O diagram (Fig. 4a), and have highly variable abundances of SiO_2, ranging from 65.9 to 74.6 wt.% (volatile free, Table 1). On a SiO_2 versus K_2O diagram (Fig. 4b), they plot from the middle of the calc alkaline field to well within the field of shoshonitic magmatic rocks. These granites have variable and high A/CNK (molar $Al_2O_3/(CaO + Na_2O + K_2O)$) values of 1.08–1.52, and plot into the strongly peraluminous field (Fig. 4c). They are characterized by strong but variable light rare earth element (REE) enrichments (La_N/Yb_N = 6.9–140) (Fig. 5a), negative Eu anomalies (one sample exhibits a positive Eu anomaly caused by plagioclase accumulation), and high field strength element (HFSE, e.g., Nb, Ta, Ti), Sr and P depletions compared with neighboring elements on multi-element "spidergrams" (Fig. 5b). The porphyritic K-feldspar granites have higher LREE contents but both types display variable MREE-HREE contents.

228

229 *4.2. Whole rock Sm–Nd isotopic compositions*

230 Eight samples were selected for whole rock Sm–Nd isotopic analyses (Table 2).
231 The porphyritic K-feldspar granites exhibit homogeneous $\varepsilon_{Nd}(t)$ values (-0.6 to +0.2)
232 (Fig. 4d), corresponding to two-stage Nd mode ages (T_{2DM}) of 2.47–2.40 Ga, whereas
233 the two-mica granites have slightly variable $\varepsilon_{Nd}(t)$ values (-1.1 to +0.9) (Fig. 4d),
234 corresponding to T_{2DM} of 2.51–2.35 Ga.

235

236 *4.3. Zircon Hf–O isotopic compositions*

237 Hafnium and oxygen isotope analyses were conducted on those zircon grains that
238 were previous analyzed for U–Pb dating (Dan et al., 2012). The ca. 1.95 Ga magmatic
239 zircon grains from samples 09AL233 and 09AL258 have $\varepsilon_{Hf}(t)$ values of -1.0 to +3.0
240 (averaged at 1.1 ± 0.8 (1SD)) and +2.1 to +8.3 (averaged at +4.9 ± 1.7 (1SD)) (Fig. 6),
241 corresponding to two-stage zircon Hf model ages (T_{DM}^{C}) of 2.66–2.41 Ga (averaged
242 at 2.53 ± 0.05 Ga (1SD)) and 2.47–2.08 Ga (averaged at 2.29 ± 0.11 Ga (1SD)),
243 respectively (Table 3).

244

245 The measured $\delta^{18}O$ values for ca. 1.95 Ga zircon grains from sample 09AL233
246 and 09AL258 show a wide range of 8.7–10.6‰ and 7.3–10.2‰, respectively (Fig. 7).
247 One grain with age of 2058 Ma from 09AL233 has a $\delta^{18}O$ value of 7.2‰ (Table 3).

248

5. Discussion

5.1. 2.0–1.8 Ga events in the Khondalite Belt

The Khondalite Belt is commonly considered to have formed at ca. 1.95 Ga (e.g., Zhao et al., 2005; Yin et al., 2009, 2011), following the termination of a ca. 2.18-2.00 Ga magmatic arc between the Yinshan and Ordos blocks (Dan et al., 2012). In order to better understand the petrogenesis and tectonic significance of the ca. 1.95 Ga event, we have summarized age data for 2.0-1.8 Ga magmatism and metamorphism in the Khondalite Belt. Owing to the rapidly growing dating database for the belt, only high-resolution ages (LA-ICP-MS and SIMS) were considered. Fig. 8 shows the frequency distribution of magmatic and metamorphic ages from the region using ISOPLOT (Ludwig, 2003). The age distribution pattern has a strong peak at 1.95 Ga and two minor peaks at 1.92 Ga at 1.84 Ga. Magmatic activities extend from 2.0 Ga to 1.8 Ga and can be divided into two main periods: 1.97-1.90 Ga and 1.89-1.82 Ga. The latter event is mainly represented by un-deformed granites and associated metamorphism and is commonly attributed to regional extension, probably during orogenic collapse (e.g., Yin et al., 2009; Jiao et al., 2013; Liu et al., 2013).

The ca. 1.97-1.90 Ga period is represented by development of diverse magmatic rocks and associated metamorphism corresponding to the earliest major igneous activity following deposition of the sedimentary protoliths of the Khondalites (ca. 2.00-1.97 Ga). This period can be roughly divided into two events, i.e., the ca. 1.97-1.95 Ga and ca. 1.93-1.90 Ga, with corresponding peak ages of ca. 1.95 Ga and

ca. 1.92 Ga, respectively (Fig. 8). The ca.1.97-1.95 Ga event is recorded by various magmatic rocks, including meta-gabbros (Wan et al., 2013a), dolerite dykes (Song et al., 2010), charnockitic gneisses (Liu et al., 2013), carbonatitic dykes (Wan et al., 2008), syenogranites (Liu et al., 2013) and S-type granites (Dan et al., 2012). The related ca. 1.95 Ga metamorphism was recorded by almost all rocks types in all complexes of the Khondalite Belt, including meta-igneous rocks (Wan et al., 2013a), meta-sedimentary rocks (Yin et al., 2009, 2011), as well as mafic and felsic granulites (Zhou and Geng, 2009; Zhou et al., 2010). The ca. 1.95 Ga metamorphic event has commonly been attributed to collision of the Yinshan and Ordos blocks (e.g., Zhao et al., 2005, 2010; Yin et al., 2009, 2011, 2014; Wang et al., 2011b; Zhao and Guo, 2012), but it is noted that the reported ca. 1.97-1.95 Ga magmatic rocks are almost entirely confined to the west-central segment of the Khondalite Belt (i.e., Helanshan and Daqingshan complexes). One possible explanation is that there is a tectonic boundary between the west-central and east segments of the Khondalite Belt (Peng et al., 2011). Another explanation is that the ca. 1.97-1.95 Ga magmatic rocks were less extensively developed toward the present-day northeast and may be covered by the extensive ca. 1.93-1.88 Ga volcanico-sedimentary sequences of the Jining Complex, whose generation has been attributed to a ridge subduction event (Peng et al., 2010, 2011, 2012).

Examples of the ca. 1.93-1.90 Ga magmatic and metamorphic events are also common features across the whole Khondalite Belt (Zhong et al., 2007; Geng et al.,

2009; Wan et al., 2009; Yin et al., 2009; Peng et al., 2010, 2011; Santosh et al., 2007a, b, 2009, 2013). Most ca. 1.93-1.92 Ga ages metamorphic ages were obtained from UHT rocks in the Jining Complex by Santosh et al. (2007a, 2007b, 2009, and 2013). The tectonic setting responsible for generation of the UHT rocks has been highly disputed and various models invoke a post-collisonal setting (Zhao, 2009; Zhao et al., 2012), slab break-off (Zhai and Santosh, 2011), a mantle plume (Santosh et al., 2010), and ridge subduction (Peng et al., 2010, 2011, 2012). This ca. 1.93-1.90 Ga event is sometimes considered to be the second stage of the ca. 1.97-1.95 Ga event, rather than a discrete episode (Liu et al., 2013), as application of the Ti-in-zircon geothermometer suggests that the peak UHT metamorphic temperature might be slightly higher than the closure temperature of zircon (Liu et al., 2010).

5.2. Source components for S-type granites

The ca. 1.95 Ga granites are one of the major rock types of the Helanshan Complex. The granites contain peraluminous minerals (i.e., muscovite), have >1% normative corundum (Table 1), and are characterized as strongly peraluminous with A/CNK values of 1.1−1.5. Samples 09AL233 and 09AL258 have similar wide ranges of zircon $\delta^{18}O$ values, 8.7–10.6 ‰ and 7.3–10.2 ‰, corresponding to calculated magmatic $\delta^{18}O$ values of 10.4–12.3 ‰ and 9.1–12.0 ‰, respectively (Lackey et al., 2008). The wide range of oxygen isotope compositions and high $\delta^{18}O$ values are typical of S-type granites (e.g., Kemp et al., 2008; Appleby et al., 2010; Dan et al., 2014). All of these lines of evidence indicate that the Helanshan granites can be

315 classified as S-type.

316

317 S-type magmas are commonly produced by partial melting of metapelites and
318 metagreywackes under water-undersaturated conditions (e.g., Vielzeuf and Holloway,
319 1988; Patiño Douce and Harris, 1998; Zhang et al., 2004; Guo and Wilson, 2012;
320 Wang et al., 2012). A series of experiments show that metasediments tend to yield
321 melts with low FeO abundances (generally < 3 wt.% FeO) despite variations in Al_2O_3
322 content (Patiño Douce and Johnston, 1991; Montel and Vielzeuf, 1997; Patiño Douce
323 and Harris, 1998; Fig. 9a). The exception is melts produced at high temperatures
324 (1050–1250 ℃) from metapelitic sources that started with a high FeO content, as
325 shown by Vielzeuf and Holloway (1988). This appears to be due to the breakdown of
326 garnet to spinel and quartz, liberating FeO into the melt (in addition to Al_2O_3, giving a
327 relatively high abundance of both elements) (Turner and Rushmer, 2009). Compared
328 to the typically metapelite-derived Himalayan leucogranites (Patiño Douce and Harris,
329 1998), the Helanshan S-type granites have higher FeO content (Fig. 9a). Thus, it
330 might be argued that the Helanshan S-type granites were derived from high
331 temperature metapelite-derived melts, which underwent plagioclase crystallization
332 (Fig. 9a). However, their low MgO contents compared to experimental
333 high-temperature melts do not support this scenario (Fig. 9b). Another possibility is
334 that another component was added to the metasediments-derived melts.
335 Mantle-derived mafic magmas generally have high FeO contents, satisfying this
336 requirement. The occurrence of contemporaneous mafic dykes in the Helanshan

Complex (Song et al., 2010) further supports this possibility.

This suggestion is also supported by the *in situ* isotopic data. In previous studies, the biotite and/or garnet-bearing granites were attributed solely to ananetic melting of Khondalite metasediments during regional metamorphism (Lu et al., 1992, 1996). The $\varepsilon_{Nd}(t)$ values of -1.1 to +0.9 obtained from the ca. 1.95 granites was considered to be evidence that they were generated by partial melting of a single juvenile sedimentary source, consistent with other S-type granites in the Khondalite Belt (e.g., Peng et al., 2012). Metasedimentary rocks of the Helanshan Complex, however, have significantly lower $\varepsilon_{Nd}(t)$ values of -7.7 to -1.2 (recalculated at 1950 Ma from Wan et al., 2000), indicating that other mantle-derived or juvenile crustal materials were added to the granites. These granites also have zircon $\varepsilon_{Hf}(t)$ values (-1.0 to +8.3) that are higher than those of ca. 1.95 Ga meta-syenogranite veins (-4.0 to +2.3) and crustal carbonatites (-3.2 to +0.7) in the Daqingshan Complex (Fig. 6) (Wan et al., 2008; Ma et al., 2012). *In-situ* zircon Hf and O isotope data further suggest that the mantle-derived or juvenile crust-derived melts contributed to the ca. 1.95 Ga S-type granites (Fig. 10), although the contribution to the porphyritic K-feldspar granite (sample 09AL233) was minor.

It is noted that there are many examples of cryptic magma mixing known from younger granites in the NCC (e.g., Sun et al., 2010), but no mafic enclaves have been discovered in those rocks. This can be explained by the fact that, like the granites of

the present study, they were highly evolved (SiO_2 = 66-71wt.%) rather than diorites or granodiorites. In such rocks, magma evolution can erase the macro-scale evidence of magma mixing, which is now only revealed by zircon Hf-O isotope studies (e.g., Appleby et al., 2008; Sun et al., 2010). Differences in terms of MgO, and SiO_2 abundances or $\varepsilon_{Nd}(t)$ and $\varepsilon_{Hf}(t)$) compositions between the porphyritic K-feldspar and two-mica granites (Figs. 4, 9 and 10) do not require that they were generated by different types of processes. Their geochemical differences can be explained in at least two ways. First, the two-mica granites may have undergone more crustal-level evolution than the porphyritic K-feldspar granites, as the former occurs as a pluton and latter as a dyke. Second, the two types of granites may have slightly different metasedimentary protolith components (e.g., Wan et al., 2000).

5.3. Geodynamics: slab break-off during ca. 1.97-1.90 Ga?

The ca. 1.95 Ga S-type granites were mainly sourced from the Khondalite metasedimentary rocks, whose protoliths are constrained to be deposition between ca. 2.00 and 1.95 Ga (Yin et al., 2011; Dan et al., 2012). As previously noted, the requirements for such rapid sedimentary recycling are only met in a few distinctive tectonic settings that involve processes such as lithospheric delamination, back-arc basin opening, mantle plume ascent or continental rifting (Li et al., 2003; Kemp et al., 2007; Zheng et al., 2008; Collins and Richards, 2008; Foster and Goscombe, 2013). A common feature of these tectonic settings is the presence of asthenosphere upwelling, consistent with the generation of high-temperature S-type granites (Sylvester, 1998).

The Helanshan Complex S-type granites can also be classified as high-temperature type. They have low Al_2O_3/TiO_2 (17-81), and plot into the "high-temperature" field (Fig. 11a), consistent with their calculated zircon saturation temperatures, which extend to ~870 ℃ (Fig. 11b, Table 1). Although several inherited zircon grains were identified during geochronological studies (Dan et al., 2012), they can only have slightly raised the calculated zircon saturation temperatures. For example, the calculated Ti-in zircon temperatures are similar to the calculated zircon saturation temperatures in the Mid-Miocene to Quaternary strongly peraluminous rhyolites in the Southern Kunlun Range (Wang et al., 2012). The high zircon saturation temperatures were also supported by the high TiO_2 contents in these samples (Fig. 11b), which are temperature dependent under conditions of uniform TiO_2 activity (Wark et al., 2007). Furthermore, the Helanshan S-type granites have distinctly higher zircon saturation temperatures than those of the Himalaya leucogranites (Fig. 11b), which were produced by fluid-present melting (e.g., Patiño Douce and Harris, 1998) or decompression melting (e.g., Guo and Wilson, 2012). Given that both the Himalaya leucogranites and Helanshan S-type granites have inherited zircons, the effects of inheritance on the zircon saturation temperatures are offset in any comparison of the two suites.

High-temperature S-type granites, formed in a high-temperature collisional orogen, are generally cordierite-bearing peraluminous granites that are considered to

403 be crust-mantle hybrids (e.g., Barbarin, 1996; Sylvester, 1998; Healy et al., 2004).
404 However, this observation does not exclude the possibility that other S-type granites
405 can be produced by mixing between mantle and crust-derived magmas. One example
406 is the Permian peraluminous granites of the Lhasa terrane (Zhu et al., 2009). The
407 inferred petrogenesis of the high temperature Helanshan S-type granites, involving
408 mixing between mantle and crust-derived magmas, further demonstrates that
409 asthenospheric upwelling is probably required to form these S-type granites (Fig. 10).
410 More direct evidence may be provided by the ca. 1.96 Ga dolerite dykes (Song et al.,
411 2010) of the Khondalite Belt, although additional geochemical data is required to
412 confirm this speculation.
413
414 The tectonic settings typically applied to high-temperature S-type granites
415 present problems if applied to the Helanshan Complex or the Khondalite Belt as a
416 whole. The Khondalite Belt is considered to have been formed at ca. 1.95 Ga (e.g.,
417 Zhao et al., 2005, 2010), which argues against back-arc extension for generating the
418 ca. 1.95 Ga magmatic rocks. Furthermore, the ca. 1.95 Ga granites in this study show
419 significant geochemical variations from mid-calc-alkaline to shoshonitic compositions,
420 implying involvement of heterogeneous mantle and/or crustal source regions in the
421 petrogenesis that is not characteristic of the main, “normal”, stage of subduction (Lee
422 et al., 2009). Similarly, lithospheric delamination models based on an active
423 subduction system, such as those found in Mesozoic North China (e.g., Wu et al.,
424 2008) and Late Paleozoic Iberia (e.g., Gutiérrez-Alonso et al., 2011), are also not

viable. The lack of plume-related rocks (high-temperature lavas, flood basalts), the linear distribution of magmatic events, and 1.97-1.90 Ga collisional setting (Jiao et al., 2013) are also inconsistent with a plume model.

Taking into account the distribution of ca. 1.97-1.90 Ga magmatic rocks in the entire Khondalite Belt, a model of slab break-off is proposed, which predicts a relatively narrow, linear zone of magmatism located along a suture zone (e.g., von Blanckenburg and Davis, 1995; Atherton and Ghani, 2002; Chung et al., 2005; Keskin et al., 2008; Xu et al., 2008; Whalen et al., 2006, 2010; Yuan et al., 2010). Several lines of evidence support this scenario. The ca. 1.95 Ga event consists of simultaneous felsic and mafic magmatism, such as the ca. 1.95 Ga S-type granites and dolerite dykes in Helanshan Complex (Song et al., 2010; Dan et al., 2012) and the ca. 1.97-1.95 Ga gabbros, syenogranites and carbonatites in Daqingshan Complex (Wan et al., 2008, 2013a; Ma et al., 2012; Liu et al., 2013). The carbonatites have characteristic enrichments in Sr, Ba and REE combined with depletions in HFSE, similar to other carbonatites emplaced in post-collisional settings (Hou et al., 2006; Chakmouradian et al., 2008). This period of magmatism was accompanied by regional ca. 1.95 Ga granulite facies metamorphism recorded by felsic and mafic granulites throughout the entire Khondalite Belt (e.g., Zhao et al., 2005, 2010; Yin et al., 2009, 2011). Finally, the tectonic setting during the ca. 1.97-1.90 Ga period was collisional or post-collisional (e.g., Jiao et al., 2013; Liu et al., 2013). The combination of contemporaneous mafic and felsic magmatism accompanied by coeval metamorphism

447 in a post-collisional orogen is similar to other Phanerozoic orogens, such as the Alps
448 (von Blanckenburg and Davis, 1995) and Tibet (Chung et al., 2005; Lee et al., 2009;
449 Jiang et al., 2014; Ma et al., 2014).
450
451 The Paleoproterozoic Khondalite Belt is probably wider than presently mapped,
452 given that Late Paleoproterozoic sedimentary rocks and metamorphism have been
453 revealed in the Ordos Block from drill core samples in recent years (Hu et al., 2012;
454 Wan et al., 2013b). Irrespective of the width that is ultimately defined, however, the
455 Khondalite Belt must represent a suture zone. Moreover, the southwest segment of the
456 Khondalite Belt must have extended into other, now removed, parts of the Columbia
457 Supercontinent (e.g., Zhao et al., 2004; Hou et al., 2008; Wang et al., 2014).
458 Accordingly, the total length of the Khondalite Belt must have originally been greater
459 than the present width of the North China Craton. The long and narrow features of the
460 proposed slab break-off model can readily explain the syn- and/or post-collisional
461 magmatism and metamorphism along the Khondalite Belt suture zone.
462
463 As previously noted, a model of ridge subduction has been proposed to account
464 for the generation of the ca. 1.93-1.92 Ga magmatic rocks and UHT metamorphism in
465 Jining Complex (Peng et al., 2010, 2011, 2012). Irrespective of the merits of this
466 model for the Jining Complex, it does not account for the similar magmatism and
467 metamorphism in the middle and southwestern parts of the Khondalite Belt, such as
468 the ca. 1.92 Ga magmatic rocks in Helanshan Complex (Geng et al., 2009), and

contemporaneous metamorphism in the Qianlishan and Daqingshan complexes (Yin et al., 2009; Ma et al., 2012). Moreover, any ridge subduction at ca. 1.93-1.90 Ga should be considered as a geodynamically distinct event from those processes associated with the generation of ca. 1.97-1.95 Ga magmatism and metamorphism along the whole 1000 km Khondalite Belt.

6. Conclusions

Based on our new data on the Helanshan Complex and previously published data for the Khondalite Belt of the North China Craton, we draw the following major conclusions:

(1) The ca. 1.95 Ga porphyritic K-feldspar granites and two-mica granites in the Helanshan Complex, North China Craton are the earliest S-type granites in the Khondalite Belt. They are peraluminous (A/CNK value >1.0), and characterized by high zircon $\delta^{18}O$ values of 7.3 to 10.6 ‰.

(2) *In situ* zircon Hf-O isotopic compositions indicate that the mantle not only supplied heat but also a magmatic component to the generation the S-type granites.

(3) A slab break-off model best explains the documented succession of events, i.e., ca. 1.97-1.76 Ga mafic magmatism, ca. 1.95-1.94 Ga mafic, carbonatitic, and S-type granitic magmatism and granulite metamorphism.

Acknowledgments

We thank Q. L. Li and G. Q. Tang for their help in SIMS analyses, Y. H. Yang for LA-MC-ICP-MS analyses, and G.C. Zhao for providing a map that is used as Fig. 1 of this paper. Thoughtful and constructive comments by two anonymous reviewers and editorial comments by G.C. Zhao substantially improved the manuscript. This study was financially supported by the Strategic Priority Research Program (B) of the Chinese Academy of Sciences (Grant no. XDB03010600), Major State Basic Research Program (973 Program) of People's Republic of China (Grant no. 2011CB808906), National Natural Science Foundation of China (Grant nos. 41025006, 41303018 and 41121002), China Postdoctoral Science Foundation (Grant no. 2013M531880), and the Guangzhou Institute of Geochemistry, Chinese Academy of Sciences (GIGCAS 135 project Y234021001). This is contribution No. IS-XXX from GIGCAS, and TIGeR (The Institute of Geoscience Research) publication No. xxx and contribution xx from the ARC Center of Excellence for Core to Crust Fluid Systems (http://www.ccfs.mq.edu.au/).

References

Appleby, S.K., Graham, C.M., Gillespie, M.R., Hinton, R.W., Oliver, G.J.H., EIMF, 2008. A cryptic record of magma mixing in diorites revealed by high-precision SIMS oxygen isotope analysis of zircons. Earth Planet. Sci. Lett. 269, 105-117.

Appleby, S.K., Gillespie, M.R., Graham, C.M., Hinton, R.W., Oliver, G.J.H., Kelly, N.M., 2010. Do S-type granites commonly sample infracrustal sources? New results from an integrated O, U–Pb and Hf isotope study of zircon. Contrib. Mineral. Petrol. 160, 115-132.

Atherton, M.P., Ghani, A.A., 2002. Slab breakoff: a model for Caledonian, Late Granite syn-collisional magmatism in the orthotectonic (metamorphic) zone of Scotland and Donegal, Ireland. Lithos 62,

65-85.
Barbarin, B., 1996. Genesis of the two main types of peraluminous granitoids. Geology 24, 295-298.
Barbarin, B., 1999. A review of the relationships between granitoid types, their origins and their geodynamic environments. Lithos 46, 605-626.
Chakmouradian, A.R., Mumin, A.H., Demény, A., Elliott, B., 2008. Postorogenic car-bonatites at Eden Lake, Trans-Hudson Orogen (northern Manitoba, Canada): geological setting, mineralogy and geochemistry. Lithos 103, 503-526.
Chung, S.L., Chu, M.F., Zhang, Y.Q., Xie, Y.W., Lo, C.H., Lee, T.Y., Lan, C.Y., Li, X.H., Zhang, Q., Wang, Y.Z., 2005. Tibetan tectonic evolution inferred from spatial and temporal variations in post-collisional magmatism. Earth-Sci. Rev. 68, 173-196.
Collins, W.J., Richards, S.W., 2008. Geodynamic significance of S-type granites in circum-Pacific orogens. Geology 36, 559-562.
Condie, K.C., Boryta, M.D., Liu, J.Z., Qian, X.L., 1992. The origin of khondalites: geochemical evidence from the Archean to Early Proterozoic granulite belt in the North China Craton. Precambrian Res. 59, 207-223.
Dan, W., Li, X.-H., Guo, J., Liu, Y., Wang, X.-C., 2012. Integrated in situ zircon U–Pb age and Hf–O isotopes for the Helanshan khondalites in North China Craton: Juvenile crustal materials deposited in active or passive continental margin? Precambrian Res. 222-223, 143-158.
Dan, W., Li, X.H., Wang, Q., Wang, X.C., Liu, Y., 2014. Neoproterozoic S-type granites in the Alxa Block, westernmost north China and tectonic implications: in-situ zircon U-Pb-Hf-O isotopic and geochemical constraints. Am. J. Sci., 314, 110-153.
Dong, C.Y., Wan, Y.S., Xu, Z.Y., Liu, D.Y., Yang, Z.S., Ma, M.Z., Xie, H.Q. 2013. SHRIMP zircon U–Pb dating of late Paleoproterozoic khondalites in the Daqing Mountain area on North China Craton.. Sci. China: Earth Sci. 56, 115-125.
Dong, C.Y., Wan, Y.S., Wilde, S.A., Xu, Z.Y., Ma, M.Z., Xie, H.Q., Liu, D.Y., 2014. Earliest Paleoproterozoic supracrustal rocks in the North China Craton recognized from the Daqingshan area of the Khondalite Belt: Constraints on craton evolution. Gondwana Res. 25, 1535-1553.
Foster, D., Goscombe, B., 2013. Continental Growth and Recycling in Convergent Orogens with Large Turbidite Fans on Oceanic Crust. Geosciences 3, 354-388.
Geng, Y.S., Zhou, X.W., Wang, X.S., Ren, L.D., 2009. Late-Paleoproterozoic granite events and their geological significance in Helanshan area, Inner Mongolia: evidence from geochronology. Acta Petrol. Sin. 25, 1830-1842 (in Chinese with English abstract).
Griffin, W.L., Pearson, N.J., Belousova, E.A., Saeed, A., 2006. Comment: Hf-isotope heterogeneity in zircon 91500. Chem. Geol. 233, 358-363.
Guo, J.H., Sun, M., Zhai, M.G., 2005. Sm-Nd and SHRIMP U-Pb zircon geochronology of high-pressure granulites in the Sanggan area, North China Craton: timing of Paleoproterozoic continental collision. J. Asian Earth Sci. 24, 629-642.
Guo, J.H., Chen, Y., Peng, P., Liu, F., Cheng, L., Zhang, L.Q. 2006. Sapphirine bearing granulite in Daqingshan, Inner Mongolia: 1.8 Ga UHT metamorphic event. In: Abstract Volume of Petrology and Earth Dynamics in China. Nanjing University, Nanjing, 215-218.
Guo, J.H., Peng, P., Chen, Y., Jiao, S.J., Windley, B.F., 2012. UHT sapphirine granulite metamorphism at 1.93–1.92Ga caused by gabbronorite intrusions: Implications for tectonic evolution of the northern margin of the North China Craton. Precambrian Res. 222-223, 124-142.
Guo, Z.F., Wilson, M., 2012. The Himalayan leucogranites: constraints on the nature of their crustal

source region and geodynamic setting. Gondwana Res. 22, 360-376.
Gutiérrez-Alonso, G., Murphy, J.B., Fernandez-Suarez, J., Weil, A.B., Franco, M.P., Gonzalo, J.C., 2011. Lithospheric delamination in the core of Pangea: Sm-Nd insights from the Iberian mantle. Geology 39, 155-158.
Healy, B., Collins, W. J., Richards, S. W., 2004. A hybrid origin for Lachlan S-type granites: the Murrumbidgee Batholith example. Lithos 78, 197-216.
Hou, Z.Q., Tian, S.H., Yuan, Z.X., Xie, Y.L., Yin, S.P., Yi, L.S., Fei, H.C., Yang, Z.M., 2006. The Himalayan collision zone carbonatites in western Sichuan, SW China: petrogenesis, mantle source and tectonic implication. Earth Planet. Sci. Lett. 244, 234-250.
Hou, G.T., Santosh, M., Qian, X.L., Lister, G., Li, J.H., 2008. Configuration of the Late Paleoproterozoic supercontinent Columbia: insights from radiating mafic dykes warms. Gondwana Res. 14, 395–409.
Hu, N.G., 1994. Evolution of Helanshan Complex. Xi'an Atlas Press, Xi'an, 1-121 pp (in Chinese with English abstract).
Hu, J.M., Liu, X.S., Li, Z.H., Zhao, Y., Zhang, S.H., Liu, X.C., Qu, H.J., Chen, H., 2012. SHRIMP U-Pb zircon dating of the Ordos Basin basement and its tectonic significance. Chin. Sci. Bull. 58, 118-127.
Jian, P., Zhang, Q., Liu, D.Y., Jin, W.J., Jia, X.Q., Qian, Q., 2005. SHRIMP dating and geological significance of Late Achaean high-Mg diorite (sanukite) and hornblende-granite at Guyang of Inner Mongolia. Acta Petrol. Sin. 21, 151-157 (in Chinese with English abstract).
Jiang, Z.Q., Wang, Q., Wyman, D. A., Li, Z. X., Yang, J. H., Shi, X.B., Ma, L., Tang, G. J., Gou, G. N., Jia, X. H., Guo, H. F., 2014. Transition from oceanic to continental lithosphere subduction in southern Tibet: Evidence from the Late Cretaceous–Early Oligocene (~ 91–30 Ma) intrusive rocks in the Chanang–Zedong area, southern Gangdese. Lithos 196-197, 213-231. .
Jiao, S.J., Guo, J.H., Harley, S.L., Peng, P., 2013. Geochronology and trace element geochemistry of zircon, monazite and garnet from the garnetite and/or associated other high-grade rocks: Implications for Palaeoproterozoic tectonothermal evolution of the Khondalite Belt, North China Craton. Precambrian Res. 237, 78-100.
King, J., Harris, N., Argles, T., Parrish, R., Zhang, H., 2011. Contribution of crustal anatexis to the tectonic evolution of Indian crust beneath southern Tibet. Geol. Soc. Am. Bull. 123, 218-239.
Lee, H.Y., Chung, S.L., Lo, C.H., Ji, J., Lee, T.Y., Qian, Q., Zhang, Q., 2009. Eocene Neotethyan slab breakoff in southern Tibet inferred from the Linzizong volcanic record. Tectonophysics 477, 20-35.
Kemp, A.I.S., Shimura, T., Hawkesworth, C.J., 2007. Linking granulites, silicic magmatism, and crustal growth in arcs: Ion microprobe (zircon) U-Pb ages from the Hidaka metamorphic belt, Japan. Geology 35, 807-810.
Kemp, A.I.S., Hawkesworth, C.J., Paterson, B.A., Foster, G.L., Kinny, P.D., Whitehouse, M.J., Maas, R., EIMF, 2008. Exploring the plutonic–volcanic link: a zircon U–Pb, Lu–Hf and O isotope study of paired volcanic and granitic units from southeastern Australia. Trans. R. Soc. Edinb: Earth Sci. 97, 337-355.
Kemp, A.I.S., Hawkesworth, C.J., Collins, W.J., Gray, C.M., Blevin, P.L., EIMF, 2009. Isotopic evidence for rapid continental growth in an extensional accretionary orogen: the Tasmanides, eastern Australia. Earth Planet. Sci. Lett. 284, 455-466.
Keskin, M., Genç, Ş.C., Tüysüz, O., 2008. Petrology and geochemistry of post-collisional Middle

Eocene volcanic units in North-Central Turkey: Evidence for magma generation by slab breakoff following the closure of the Northern Neotethys Ocean. Lithos 104, 267-305.

Kretz, R., 1983. Symbols for rock-forming minerals. Am. Mineral. 68, 277-279.

Kröner, A., Wilde, S.A., Li, J.H., Wang, K.Y., 2005. Age and evolution of a late Archaean to early Paleozoic upper to lower crustal section in the Wutaishan/Hengshan/Fuping terrain of northern China. J. Asian Earth Sci. 24, 577-595.

Kusky, T.M., Li, J.H., 2003. Paleoproterozoic tectonic evolution of the North China Craton. J. Asian Earth Sci. 22, 383-397.

Kusky, T.M., Li, J.H., Santosh, M., 2007. The Paleoproterozoic North Hebei Orogen: North China Craton's collisional suture with the Columbia Supercontinent. Gondwana Res. 12, 4-28.

Lackey, J.S., Valley, J.W., Chen, J.H., Stockli, D.F., 2008. Dynamic magma systems, crustal recycling, and alteration in the central Sierra Nevada Batholith: the oxygen isotope record. J. Petrol. 49,1397-1426.

Li, S.Z., Zhao, G.C., 2007. SHRIMP U-Pb zircon geochronology of the Liaoji granitoids: constraints on the evolution of the Paleoproterozoic Jiao-Liao-Ji belt in the Eastern Block of the North China Craton. Precambrian Res. 158, 1-16.

Li, X.H., Sun, M., Wei, G.J., Liu, Y., Lee, C.Y., Malpas, J., 2000. Geochemical and Sm-Nd isotopic study of amphibolites in the Cathaysia Block, southeastern China: evidence for an extremely depleted mantle in the Paleoproterozoic. Precambrian Res. 102, 251-262.

Li, X.H., Li, Z.X., Ge, W., Zhou, H., Li, W., Liu, Y., Wingate, M.T.D., 2003. Neoproterozoic granitoids in South China: crustal melting above a mantle plume at ca. 825 Ma? Precambrian Res. 122, 45-83.

Li, S.Z., Zhao, G.C., Sun, M., Wu, F.Y., Liu, J.Z., Hao, D.F., Han, Z.Z., Luo, Y., 2004a. Mesozoic, not Paleoproterozoic SHRIMP U-Pb zircon ages of two Liaoji granites, Eastern Block, North China Craton. Int. Geol. Rev. 46, 162-176.

Li, X.H., Liu, D.Y., Sun, M., Li, W.X., Liang, X.R., Liu, Y., 2004b. Precise Sm-Nd and U-Pb isotopic dating of the supergiant Shizhuyuan polymetallic deposit and its host granite, SE China. Geol. Mag. 141, 225-231.

Li, S.Z., Zhao, G.C., Sun, M., Han, Z.Z., Luo, Y., Hao, D.F., Xia, X.P., 2005a. Deformation history of the Paleoproterozoic Liaohe assemblage in the eastern block of the North China Craton. J. Asian Earth Sci. 24, 659-674.

Li, X.H., Qi, C.S., Liu, Y., Liang, X.R., Tu, X.L., Xie, L.W., Yang, Y.H., 2005b. Petrogenesis of the Neoproterozoic bimodal volcanic rocks along the western margin of the Yangtze Block: New constraints from Hf isotopes and Fe/Mn ratios. Chin. Sci. Bull. 50, 2481-2486.

Li, S.Z., Zhao, G.C., Sun, M., Han, Z.Z., Zhao, G.T., Hao, D.F., 2006. Are the South and North Liaohe Groups of the North China Craton different exotic terranes? Nd isotope constraints. Gondwana Res. 9, 198-208.

Li, S.Z., Zhao, G.C., Zhang, J., Sun, M., Zhang, G.W., Luo, D., 2010a. Deformational history of the Hengshan-Wutai-Fuping belt: Implications for the evolution of the Trans-North China Orogen. Gondwana Res. 18, 611-631.

Li, X.H., Li, W.X., Li, Q.L., Wang, X.C., Liu, Y., Yang, Y.H., 2010b. Petrogenesis and tectonic significance of the ~850 Ma Gangbian alkaline complex in South China: evidence from in situ zircon U-Pb dating, Hf-O isotopes and whole-rock geochemistry. Lithos 114, 1-15.

Li, X.H., Long, W.G., Li, Q.L., Liu, Y., Zheng, Y.F., Yang, Y.H., Chamberlain, K.R., Wan, D.F., Guo,

C.H., Wang, X.C., Tao, H., 2010c. Penglai zircon megacrysts: a potential new working reference material for microbeam determination of Hf-O isotopes and U-Pb age. Geostand. Geoanal. Res. 34, 117-134.

Li, X.P., Yang, Z.Y., Zhao, G.C., Grapes, R., Guo, J.H., 2011a. Geochronology of khondalite-series rocks of the Jining Complex: confirmation of depositional age and tectonometamorphic evolution of the North China craton. Int. Geol. Rev. 53, 1194-1211.

Li, S.Z., Zhao, G.C., Santosh, M., Liu, X.,Dai, L.M., 2011b. Palaeoproterozoic tectonothermal evolution and deep crustal processes in the Jiao-Liao-Ji Belt, North China Craton: a review. Geol. J. 46, 525-543.

Li, S.Z., Zhao, G.C., Santosh, M., Liu, X., Lai, L.M., Suo, Y.H., Song, M.C., Wang, P.C., 2012. Paleoproterozoic structural evolution of the southern segment of the Jiao-Liao-Ji Belt, North China Craton. Precambrian Res. 200-203, 59-73.

Liu, S.J., Li, J.H., Santosh, M., 2010. First application of the revised Ti-in-zircon geothermometer to Paleoproterozoic ultrahigh-temperature granulites of Tuguiwula, Inner Mongolia, North China Craton. Contrib. Mineral. Petrol. 159, 225-235.

Liu, S.J., Tsunogae, T., Li, W.S., Shimizu, H., Santosh, M., Wan, Y.S., Li, J.H. 2012a. Paleoproterozoic granulites from Heling'er: implications for regional ultrahigh-temperature metamorphism in the North China Craton. Lithos 148, 54-70.

Liu, C.H., Zhao, G.C., Sun, M., Liu, F.L., Zhang, J., Yin, C.Q., 2012b. Zircons U-Pb and Lu-Hf isotopic and whole-rock geochemical constraints on the Gantaohe Group in the Zanhuang Complex: Implications for the tectonic evolution of the Trans-North China Orogen. Lithos 146-147, 80-92.

Liu, C.H., Zhao, G.C., Sun, M., Zhang, J., Yin, C.Q., 2012c. U-Pb geochronology and Hf isotope geochemistry of detrital zircons from the Zhongtiao Complex: Constraints on the tectonic evolution of the Trans-North China Orogen. Precambrian Res. 222-223, 159-172.

Liu, C.H., Zhao, G.C., Sun, M., Zhang, J., Yin, C.Q., He, Y.H., 2012d. Detrital zircons U-Pb dating, Hf isotope and whole-rock geochemistry from the Songshan Group in the Dengfeng Complex: Constraints on the tectonic evolution of the Trans-North China Orogen. Precambrian Res. 192-195, 1-15.

Liu, S.J., Dong, C.Y., Xu, Z.Y., Santosh, M., Ma, M.Z., Xie, H.Q., Liu, D.Y., Wan, Y.S., 2013. Palaeoproterozoic episodic magmatism and high-grade metamorphism in the North China Craton: evidence from SHRIMP zircon dating of magmatic suites in the Daqingshan area. Geol. J. 48, 429-455.

Liu, P.H., Liu, F.L., Liu, C.H., Liu, J.H., Wang, F., Xiao, L.L., Cai, J., Shi, J.R., 2014. Multiple mafic magmatic and high-grade metamorphic events revealed by zircons from meta-mafic rocks in the Daqingshan−Wulashan Complex of the Khondalite Belt, North China Craton. Precambrian Res. 246, 334-357.

Lu, L.Z., Jin, S.Q., Xu, X.C., Liu, F.L., 1992. Petrogenesis of Early Precambrian khondalite series in Southeastern Inner Mongolia and its potential mineral resources. Jilin Sci. Tech. Press, Changchun, 1-156 pp (in Chinese with English abstract).

Lu, L.Z., Xu, X.C., Liu, F.L., 1996. Early Precambrian Khondalite series of North China. Changchun Publ. House, Changchun, pp. 1-272 (in Chinese).

Lu, S.N., Zhao, G.C., Wang, H.C, Hao, G.J, 2008. Precambrian metamorphic basement and sedimentary cover of the North China Craton: A review. Precambrian Res. 160, 77-93.

Ludwig, K.R., 2003. Users Manual for Isoplot 3.00: A Geochronological Toolkit for Microsoft Excel:

692 Berkeley Geochronology Center, Special Publication, 4.
693 Luo, Y., Sun, M., Zhao, G.C., Li, S.Z., Xu, P., Ye, K., Xia, X.P., 2004. LA-ICP-MS U-Pb zircon ages of
694 the Liaohe Group in the Eastern Block of the North China Craton: constraints on the evolution of
695 the Jiao-Liao-Ji Belt. Precambrian Res. 134, 349-371.
696 Luo, Y., Sun, M., Zhao, G.C., Ayers, J.C., Li, S.Z., Xia, X.P., Zhang, J.H., 2008. A comparison of U-Pb
697 and Hf isotopic compositions of detrital zircons from the North and South Liaohe Group:
698 Constraints on the evolution of the Jiao-Liao-Ji Belt, North China Craton. Precambrian Res. 163,
699 279-306.
700 Ma, M.Z., Wan, Y.S., Santosh, M., Xu, Z.Y., Xie, H.Q., Dong, C.Y., Liu, D.Y., Guo, C.L., 2012.
701 Decoding multiple tectonothermal events in zircons from single rock samples: SHRIMP zircon
702 U–Pb data from the late Neoarchean rocks of Daqingshan, North China Craton. Gondwana Res.
703 22, 810-827.
704 Ma, L., Wang, B. D., Jiang, Z. Q., Wang, Q., Li, Z. X., Wyman, D. A., Zhao, S. R., Yang, J. H., Gou,
705 G. N., Guo, H. F., 2014. Petrogenesis of the Early Eocene adakitic rocks in the Napuri area,
706 southern Lhasa: partial melting of thickened lower crust during slab break-off and implications
707 for crustal thickening in southern Tibet. Lithos 196-197, 321-338.
708 Montel, J.M., Vielzeuf, D., 1997. Partial melting of metagreywackes. Part : compositions of minerals
709 and melts. Contrib. Mineral. Petrol. 128, 176-196.
710 Patiño Douce, A.E., Johnston, A., 1991. Phase equilibria and melt productivity in the granulites.
711 Contrib. Mineral. Petrol. 107, 202-218.
712 Patiño Douce, A.E., Harris, N., 1998. Experimental constraints on Himalayan anatexis. J. Petrol. 39,
713 689-710.
714 Peng, P., Guo, J.H., Zhai, M.G.., Bleeker, W., 2010. Paleoproterozoic gabbronoritic and granitic
715 magmatism in the northern margin of the North China craton: Evidence of crust-mantle interaction.
716 Precambrian Res. 183, 635-659.
717 Peng, P., Guo, J.H., Windley, B.F., Li, X.H., 2011. Halaqin volcano-sedimentary succession in the
718 central-northern margin of the North China Craton: products of Late Paleoproterozoic ridge
719 subduction. Precambrian Res. 187, 165-180.
720 Peng, P., Guo, J.H., Windley, B.F., Liu, F., Chu, Z., Zhai, M.G., 2012. Petrogenesis of Late
721 Paleoproterozoic Liangcheng charnockites and S-type granites in the central-northern margin of
722 the North China Craton: Implications for ridge subduction. Precambrian Res. 222-223, 107-123.
723 Santosh, M., Tsunogae, T., Li, J.H., Liu, S.J., 2007a. Discovery of sapphirine-bearing Mg–Al granulites
724 in the North China Craton: Implications for Paleoproterozoic ultrahigh temperature metamorphism.
725 Gondwana Res. 11, 263-285.
726 Santosh, M., Wilde, S., Li, J., 2007b. Timing of Paleoproterozoic ultrahigh-temperature metamorphism
727 in the North China Craton: Evidence from SHRIMP U–Pb zircon geochronology. Precambrian
728 Res. 159, 178-196.
729 Santosh, M., Wan, Y., Liu, D., Chunyan, D., Li, J., 2009. Anatomy of Zircons from an Ultrahot Orogen:
730 The Amalgamation of the North China Craton within the Supercontinent Columbia. J. Geol. 117,
731 429-443.
732 Santosh, M., Zhao, D.-P., Kusky, T., 2010. Mantle dynamics of the Paleoproterozoic North China
733 Craton: a perspective based on seismic tomography. J. Geodyn. 49, 39-53.
734 Santosh, M., Liu, D., Shi, Y., Liu, S.J., 2013. Paleoproterozoic accretionary orogenesis in the North
735 China Craton: A SHRIMP zircon study. Precambrian Res. 227, 29-54.

Song, X.H., Li. H.Y., Guo, H.W., Zhang, L.C., Sun, W.K., Gu, S.J., Chen, Z.G., Zhang, X.J., 2010. Original rocks, ages and its significance for the wall rock of Niutougou gold deposit in northern Helan Mountains. Acta Petrol. Sin. 26, 1625-1632.

Sun, S.-S., McDonough, W.F., 1989. Chemical and isotopic systematics of oceanic basalts implications for mantle composition and process. In: Saunders, A.D., Norry, M.J. (Eds.), Magmatism in the Ocean Basins, vol. 42. Geol. Soc., London, pp. 313–354 (Spec. Pub.).

Sun, J.F., Yang, J.H., Wu, F.Y., Li, X.H., Yang, Y.H., Xie, L.W., Wilde, S.A., 2010. Magma mixing controlling the origin of the Early Cretaceous Fangshan granitic pluton, North China Craton: In situ U–Pb age and Sr-, Nd-, Hf- and O-isotope evidence. Lithos 120, 421-438.

Sylvester, P.J., 1998. Post-collisional strongly peraluminous granites. Lithos 45, 29–44.

Tam, P.Y., Zhao, G.C., Liu, F.L., Zhou, X.W., Sun, M., Li, S.Z., 2011. SHRIMP U-Pb zircon ages of high-pressure mafic and pelitic granulites and associated rocks in the Jiaobei massif: Constraints on the metamorphic ages of the Paleoproterozoic Jiao-Liao-Ji Belt in the North China Craton. Gondwana Res. 19, 150–162.

Tam, P.Y., Zhao, G.C., Sun, M. Li, S.Z., Iizukac, Y., Ma, S.K., yin, C.Q., He, Y.H., Wu, M.L., 2012a. Metamorphic P-T path and tectonic implications of medium-pressure pelitic granulites from the Jiaobei massif in the Jiao-Liao-Ji Belt, North China Craton. Precambrian Res. 220-221, 177-191.

Tam, P.Y., Zhao, G.C., Zhou, X.W., Sun, M., Li, S.Z., Yin, C.Q., Wu, M.L., He, Y.H., 2012b. Metamorphic P–T path and implications of high-pressure pelitic granulites from the Jiaobei massif in the Jiao-Liao-Ji Belt, North China Craton. Gondwana Res. 22, 104-117.

Tam, P.Y., Zhao, G.C., Sun, M., Li, S.Z., Wu, M.L., Yin, C.Q., 2012c. Petrology and metamorphic P-T path of high-pressure mafic granulites from the Jiaobei massif in the Jiao-Liao-Ji Belt, North China Craton. Lithos 155, 94-109.

Trap, P., Faure, M., Lin, W., Monié, P., 2007. Late Paleoproterozoic (1900–1800 Ma) nappe stacking and polyphase deformation in the Hengshan–Wutaishan area: Implications for the understanding of the Trans-North-China Belt, North China Craton. Precambrian Res. 156, 85–106.

Turner, S.P., Rushmer, T., 2009. Similarities between mantle-derived A-type granites and voluminous rhyolites in continental flood basalts provinces. Earth Environ. Sci. Trans. R. Soc. Edinb. 100, 1-10.

Vielzeuf, D., Holloway, J.R, 1988. Experimental determination of the fluid-absent melting relations in the pelitic system. Contrib. Mineral. Petrol. 98, 257-276.

Visonà, D., Lombardo, B., 2002. Two-mica and tourmaline leucogranites from the Everest-Makalu region (Nepal-Tibet). Himalayan leucogranite genesis by isobaric heating? Lithos 62, 125-150.

von Blanckenburg, F., Davis, J.H., 1995. Slab breakoff: a model for syncollisional magmatism and tectonics in the Alps. Tectonics 14, 120-131.

Watson, E.B., Harrison, T.M., 1983. Zircon saturation revisited: temperature and composition effects in a variety of crustal magma types. Earth Planet. Sci. Lett. 64, 295-304.

Wark, D.A., Hildreth, W., Spear, F.S., Cherniak, D.J., Watson, E.B., 2007. Pre-eruption recharge of the Bishop magma chamber. Geology 35, 235–238.

Wan, Y.S., Geng, Y.S., Liu, F.L., Shen, Q.H., Liu, D.Y., Song, B., 2000. Age and composition of the khondalite series of the North China Craton and its adjacent area. Prog. Precambrian Res. 23, 221-235 (in Chinese with English abstract).

Wan, Y.S., Song, B., Liu, D.Y., Wilde, S.A., Wu, J.S., Shi, Y.R., Yin, X.Y., Zhou, H.Y., 2006. SHRIMP U-Pb zircon geochronology of Palaeoproterozoic metasedimentary rocks in the North China

Craton: evidence for a major Late Palaeoproterozoic tectonothermal event. Precambrian Res. 149, 249-271.

Wan, Y.S., Liu, D.Y., Xu, Z.Y., Dong, C.Y., Wang, Z.J., Zhou, H.Y., Yang, Z.S., Liu, Z.H., Wu, J.S., 2008. Paleoproterozoic crustally derived carbonate-rich magmatic rocks from the Daqinshan area, North China Craton: Geological, petrographical, geochronological and geochemical (Hf, Nd, O and C) evidence. Am. J. Sci. 308, 351-378.

Wan, Y.S., Liu, D.Y., Dong, C.Y., Xu, Z.Y., Wang, Z.J., Wilde, S.A., Yang, Y.H., Liu, Z.H., Zhou, H.Y., 2009. The Precambrian Khondalite Belt in the Daqingshan area, North China Craton: evidence for multiple metamorphic events in the Palaeoproterozoic era. In: Reddy, S.M., Mazumder, R., Evans, D.A.D., Collins, A.S. (eds.), Palaeoproterozoic Supercontinents and Global Evolution. Geol. Soc. London, Spec. Publ. 323, pp.73-97.

Wan, Y., Xu, Z., Dong, C., Nutman, A., Ma, M., Xie, H., Liu, S., Liu, D., Wang, H., Cu, H., 2013a. Episodic Paleoproterozoic (～2.45, ～1.95 and ～1.85Ga) mafic magmatism and associated high temperature metamorphism in the Daqingshan area, North China Craton: SHRIMP zircon U–Pb dating and whole-rock geochemistry. Precambrian Res. 224, 71-93.

Wan, Y.S., Xie, H.Q., Yang, H., Wang, Z.J., Liu, D.Y., Kröner, A., Wilde, S.A., Geng, Y.S., Sun, L.Y., Ma, M.Z., Liu, S.J., Dong, C.Y., Du, L.L., 2013b. Is the Ordos Block Archean or Paleoproterozoic in age? Implications for the Precambrian evolution of the North China Craton. Ameri. J. Sci. 313, 683-711.

Wang, J., Wu, Y.B., Gao, S., Peng, M., Liu, X.C., Zhao, L.S., Zhou, L., Hu, Z.C., Gong, H.J., Liu, Y.S., 2010a. Zircon U-Pb and trace element data from rocks of the Huai'an Complex: new insights into the late Paleoproterozoic collision between the Eastern and Western Blocks of the North China Craton. Precambrian Res. 178, 59-71.

Wang, Z.H., Wilde, S.A., Wan, J.L., 2010b. Tectonic setting and significance of 2.3-2.1 Ga magmatic events in the Trans-North China Orogen: new constraints from the Yanmenguan mafic-ultramafic intrusion in the Hengshan-Wutai-Fuping area. Precambrian Res. 178, 27-42.

Wang, H., Wu, Y.B., Gao, S., Zhang, H.F., Liu, X.C., Gong, H.J., Peng, M., Wang, J., Yuan, H.L., 2011a. Silurian granulite-facies metamorphism, and coeval magmatism and crustal growth in the Tongbai orogen, central China. Lithos 125, 249-271.

Wang, F., Li, X.P., Chu, H., Zhao, G.C., 2011b. Petrology and metamorphism of khondalites from Jining Complex in the North China Craton. Int. Geol. Rev. 53, 212-229.

Wang, Q., Chung, S.L., Li, X.H., Wyman, D., Li, Z.X., Sun, W.D., Qiu, H.N., Liu, Y.S., Zhu, Y.T., 2012. Crustal melting and flow beneath northern Tibet: Evidence from Mid-Miocene to Quaternary strongly peraluminous rhyolites in southern Kunlun Range. J. Petrol. 53, 2523-2566.

Wang, W., Liu, S., Santosh, M., Zhang, L., Bai, X., Zhao, Y., Zhang, S., Guo, R., 2014. 1.23 Ga mafic dykes in the North China Craton and their implications for the reconstruction of the Columbia supercontinent. Gondwana Res. doi:10.1016/j.gr.2014.02.002.

Whalen, J.B., McNicoll, V.J., van Staal, C.R., Lissenberg, C.J., Longstaffe, F.J., Jenner, G.A., van Breeman, O., 2006. Spatial, temporal and geochemical characteristics of Silurian collision-zone magmatism, Newfoundland Appalachians: An example of a rapidly evolving magmatic system related to slab break-off. Lithos 89, 377-404.

Whalen, J.B., Wodicka, N., Taylor, B.E., Jackson, G.D., 2010. Cumberland batholith, Trans-Hudson Orogen, Canada: Petrogenesis and implications for Paleoproterozoic crustal and orogenic processes. Lithos 117, 99-118.

Wiedenbeck, M., Hanchar, J.M., Peck, W.H., Sylvester, P., Valley, J., Whitehouse, M., Kronz, A., Morishita, Y., Nasdala, L., Fiebig, J., Franchi, I., Girard, J.P., Greenwood, R.C., Hinton, R., Kita, N., Mason, P.R.D., Norman, M., Ogasawara, M., Piccoli, R., Rhede, D., Satoh, H., Schulz-Dobrick, B., Skar, O., Spicuzza, M.J., Terada, K., Tindle, A., Togashi, S., Vennemann, T., Xie, Q., Zheng, Y.F., 2004. Further characterisation of the 91500 zircon crystal. Geostand. Geoanal. Res. 28, 9-39.

Wu, F.Y., Yang, Y.H., Xie, L.W., Yang, J.H., Xu, P., 2006. Hf isotopic compositions of the standard zircons and baddeleyites used in U-Pb geochronology. Chem. Geol. 234, 105-126.

Wu, F.Y., Xu, Y.G., Gao, S., Zheng, J.P., 2008. Lithospheric thinning and destruction of the North China Craton. Acta Petrol. Sin. 24, 1145-1174.

Xia, X.P., Sun, M., Zhao, G.C., Luo, Y., 2006a. LA-ICP-MS U-Pb geochronology of detrital zircons from the Jining Complex, North China Craton and its tectonic significance. Precambrian Res. 144, 199-212.

Xia, X.P., Sun, M., Zhao, G.C., Wu, F.Y., Xu, P., Zhang, J.H., Luo, Y., 2006b. U-Pb and Hf isotopic study of detrital zircons from the Wulashan khondalites: constraints on the evolution of the Ordos Terrane, Western block of the North China Craton. Earth Planet. Sci. Lett. 241, 581-593.

Xia, X.P., Sun, M., Zhao, G.C., Wu, F.Y., Xu, P., Zhang, J.S., 2008. Paleoproterozoic crustal growth events in the Western Block of the North China Craton: Evidence from detrital zircon Hf and whole rock Sr-Nd isotopes of the khondalites in the Jining Complex. Am. J. Sci. 308, 304-327.

Xia, X.P., Sun, M., Zhao, G.C., Wu, F.Y., Xie, L.W., 2009. U - Pb and Hf isotopic study of detrital zircons from the Lüliang khondalite, North China Craton, and their tectonic implications. Geol. Mag. 146, 701-716.

Xu, Y.G., Lan, J.B., Yang, Q.J., Huang, X.L., Qiu, H.N., 2008. Eocene break-off of the Neo-Tethyan slab as inferred from intraplate-type basaltic dykes in the Gaoligong belt, eastern Tibet. Chem. Geol. 255, 439-453.

Yin, C.Q., Zhao, G.C., Sun, M., Xia, X.P., Wei, C.J., Zhou, X.W., Leung, W.H., 2009. LA-ICP-MS U-Pb zircon ages of the Qianlishan Complex: constrains on the evolution of the Khondalite Belt in the Western Block of the North China Craton. Precambrian Res. 174, 78-94.

Yin, C.Q., Zhao, G.C., Guo, J.H., Sun, M., Xia, X.P., Zhou, X.W., Liu, C.H., 2011. U–Pb and Hf isotopic study of zircons of the Helanshan Complex: constrains on the evolution of the Khondalite Belt in the Western Block of the North China Craton. Lithos 122, 25-38.

Yin, C.Q., Zhao, G.C., Wei, C.J., Sun, M., Guo, J.H., Zhou, X.W., 2014. Metamorphism and partial melting of high-pressure pelitic granulites from the Qianlishan Complex: Constraints on the tectonic evolution of the Khondalite Belt in the North China Craton. Precambrian Res. 242, 172-186.

Yuan, C., Sun, M.,Wilde, S., Xiao,W.J., Xu, Y.G., Long, X.P., Zhao, G.C., 2010. Post-collisional plutons in the Balikun area, East Chinese Tianshan: evolving magmatism in response to extension and slab break-off. Lithos 119, 269-288.

Zhai, M.G., Santosh, M., 2011. The early Precambrian odyssey of North China Craton: a synoptic overview. Gondwana Res. 20, 6-25.

Zhang, H.F., Harris, N., Parrish, R., Kelley, S., Zhang, L., Rogers, N., Argles, T., King, J., 2004. Causes and consequences of protracted melting of the mid-crust exposed in the North Himalayan antiform. Earth Planet. Sci. Lett. 228, 195-212.

Zhang, J., Zhao, G.C., Li, S.Z., Sun, M., Liu, S.W., Wilde, S.A., Kröner, A., Yin, C.Q., 2007.

Deformation history of the Hengshan Complex: implications for the tectonic evolution of the Trans-North China Orogen. J. Struct. Geol. 29, 933-949.

Zhang, J., Zhao, G.C., Li, S.Z., Sun, M., Wilde, S.A., Liu, S.W., Yin, C.Q., 2009. Polyphase deformation of the Fuping Complex, Trans-North China Orogen: structures, SHRIMP U–Pb zircon ages and tectonic implications. J. Struct. Geol. 31, 177-193.

Zhang, H.T., Li, J.H., Liu, S.J., Li, W.S., Santosh, M., Wang, H.H., 2012a. Spinel + quartz-bearing ultrahigh-temperature granulites from Xumayao, Inner Mongolia Suture Zone, North China Craton: petrology, phase equilibria and counterclockwise P–T path. Geosci. Front. 3, 603-611.

Zhang, J., Zhao, G.C., Shen, W.L., Li, S.Z., Sun, M., Chan, L.S., Liu, S.W., 2012b. Structural and aeromagnetic studies of the Wutai Complex: Implications for the Tectonic Evolution of the Trans-North China Orogen. Precambrian Res. 222-223, 212-229.

Zhao, G.C., Wilde, S.A., Cawood, P.A., Lu, L.Z., 1999. Tectonothermal history of the basement rocks in the western zone of the North China Craton and its tectonic implications. Tectonophysics 310, 37-53.

Zhao, G.C., Wilde, S.A., Cawood, P.A., Sun, M., 2001. Archean blocks and their boundaries in the North China Craton: lithological, geochemical, structural and P-T path constraints and tectonic evolution. Precambrian Res. 107, 45-73.

Zhao, G.C., Sun, M., Wilde, S.A., Li, S.Z., 2004. A Paleo-Mesoproterozoic supercontinent: Assembly, growth and breakup. Earth-Sci. Revi. 67, 91–123.

Zhao, G.C., Sun, M., Wilde, S.A., Li, S.Z., 2005. Late Archean to Paleoproterozoic evolution of the North China Craton: key issues revisited. Precambrian Res. 136, 177-202.

Zhao, G.C., 2009. Metamorphic evolution of major tectonic units in the basement of the North China Craton: key issues and discussion. Acta Petrol. Sin. 25, 1772-1792 (in Chinese with English abstract).

Zhao, G.C., 2014. Precambrian evolution of the North China Craton. Elsevier, Amsterdam, 194p.

Zhao, G.C., Cawood, P.A., 2012. Precambrian Geology of China. Precambrian Res. 222-223, 13-54.

Zhao, G.C., Guo, J.H., 2012. Precambrian Geology of China: Preface. Precambrian Res. 222-223, 1-12.

Zhao, G.C., Zhai, M.G., 2013. Lithotectonic elements of Precambrian basement in the North China Craton: review and tectonic implications. Gondwana Res. 23, 1207-1240.

Zhao, G.C., Wilde, S.A., Guo, J.H., Cawood, P.A., Sun, M., Li, X.P., 2010. Single zircon grains record two Paleoproterozoic collisional events in the North China Craton. Precambrian Res. 177, 266-276.

Zhao, G.C., Cawood, P.A., Wilde, S.A., Sun, M., Zhang, J., He, Y.H., Yin, C.Q., 2012. Amalgamation of the North China Craton: key issues and discussion. Precambrian Res. 222-223, 55-76.

Zheng, Y.-F., Wu, R.-X., Wu, Y.-B., Zhang, S.-B., Yuan, H., Wu, F.-Y., 2008. Rift melting of juvenile arc-derived crust: Geochemical evidence from Neoproterozoic volcanic and granitic rocks in the Jiangnan Orogen, South China. Precambrian Res. 163, 351-383.

Zhong, C.T., Deng, J.F., Wan, Y.S., Mao, D.B., Li, H.M., 2007. Magma recording of Paleoproterozoic orogeny in central segment of northern margin of North China craton: geochemical characteristics and zircon SHRIMP dating of S-type granitoids. Geochimica 36, 633-637 (in Chinese with English abstract).

Zhou, X.W., Geng, Y.S., 2009. Metamorphic age of the khondalites in the Helanshan region: constraints on the evolution of the Western block in the North China Craton. Acta Petrol. Sin. 25, 1843-1852 (in Chinese with English abstract).

912 Zhou, X.W., Zhao, G.C., Wei, C.J., Geng, Y.S., Sun, M., 2008. Metamorphic evolution and Th-U-Pb
913 zircon and monazite geochronology of high-pressure pelitic granulites in the Jiaobei massif of the
914 North China Craton. Am. J. Sci. 308 328-350.
915 Zhou, X.W., Zhao, G.C., Geng, Y.S., 2010. Helanshan high-pressure pelitic granulites: petrological
916 evidence for collision event in the Western Block of the North China Craton. Acta Petrol. Sin. 26,
917 2113-2121 (in Chinese with English abstract).
918 Zhu, D.C., Mo, X.X., Niu, Y.L., Zhao, Z.D., Wang, L.Q., Pan, G.T., Wu, F.Y., 2009. Zircon U-Pb
919 dating and in-situ Hf isotopic analysis of Permian peraluminous granite in the Lhasa terrane,
920 southern Tibet: Implications for Permian collisional orogeny and paleogeography.
921 Tectonophysics 469, 48-60.

922

Figiure captions

Fig. 1 Tectonic subdivision of the North China Craton (Zhao et al., 2005; Zhao et al., 2012). Abbreviations for metamorphic complexes in the Khondalite Belt: DU, Daqingshan-Ulashan; HL, Helanshan; JN, Jining; QL, Qianlishan.

Fig. 2 Simplified geological map of the Helanshan Complex.

Fig. 3 Field photograph and photomicrographs for the Helanshan granites. (a, c) porphyritic K-feldspar granite, (b, d) two-mica granite. The mineral abbreviations are after Kretz (1983). The (a) and (c) are reproduced from Dan et al., 2012.

Fig. 4 Diagrams of (a) SiO_2 vs. K_2O+Na_2O, (b) SiO_2 vs. K_2O , (c) A/CNK vs. A/NK, and (d) SiO_2 vs. $\varepsilon_{Nd}(t)$ values.

Fig. 5 Chondrite-normalized REE diagrams (a) and (b) primitive mantle-normalized incompatible trace element spidergrams for the granites. The normalization values are from Sun and McDonough (1989).

Fig. 6 Plot of $\varepsilon_{Hf}(t)$ values vs. zircon ages for the Paleoproterozoic rocks in Khondalite Belt. Data sources: carbonatite, Wan et al., 2008; syenogranite, Ma et al., 2012.

Fig. 7 Probability plots of zircon $\delta^{18}O$ values for the Paleoproterozoic granites.

Fig. 8 Cumulative age spectra for the ca. 2.0-1.8 Ga ages from the Khondalite Belt. Data sources are in Supplementary Table A.1.

951 Fig. 9 Plots of (a) Al_2O_3 vs. FeO and (b) MgO vs. SiO_2. Metasediments
952 experimental data, light shaded area: Patiño Douce and Johnston, 1991;
953 Montel and Vielzeuf, 1997; Patiño Douce and Harris, 1998; dark shaded area:
954 Vielzeuf and Holloway, 1988. Data for the Himalayan leucogranites: Visonà
955 and Lombardo, 2002; Zhang et al., 2004; King et al., 2011; Guo and Wilson,
956 2012, and references therein.
957
958 Fig. 10 Plot of zircon $\varepsilon_{Hf}(t)$ values vs. $\delta^{18}O$ values. The dashed lines denote the
959 two-component mixing trends between the mantle- and supracrust-derived
960 magmas. Hf_{pm}/Hf_c is the ratio of Hf concentration in the parental mantle
961 magma (pm) over crustal (c) melt indicated for each curves, and the small
962 rhombuses and ticks on the curves represent 10% mixing increments by
963 arbitrary assuming the mantle zircon has $\varepsilon_{Hf} = 10$ and $\delta^{18}O = 5.3‰$, and
964 crustal zircon = -1 and $\delta^{18}O = 10.6‰$, respectively.
965
966 Fig. 11 (a) CaO/Na_2O vs. Al_2O_3/TiO_2 diagram for the granites. The data for fields of
967 high-temperature and high-pressure collisional orogens are compiled by
968 Sylvester, 1998. (b) SiO_2 vs. Temperature for the granites. Data sources for
969 the Himalayan leucogranites are the same as in Fig. 9.

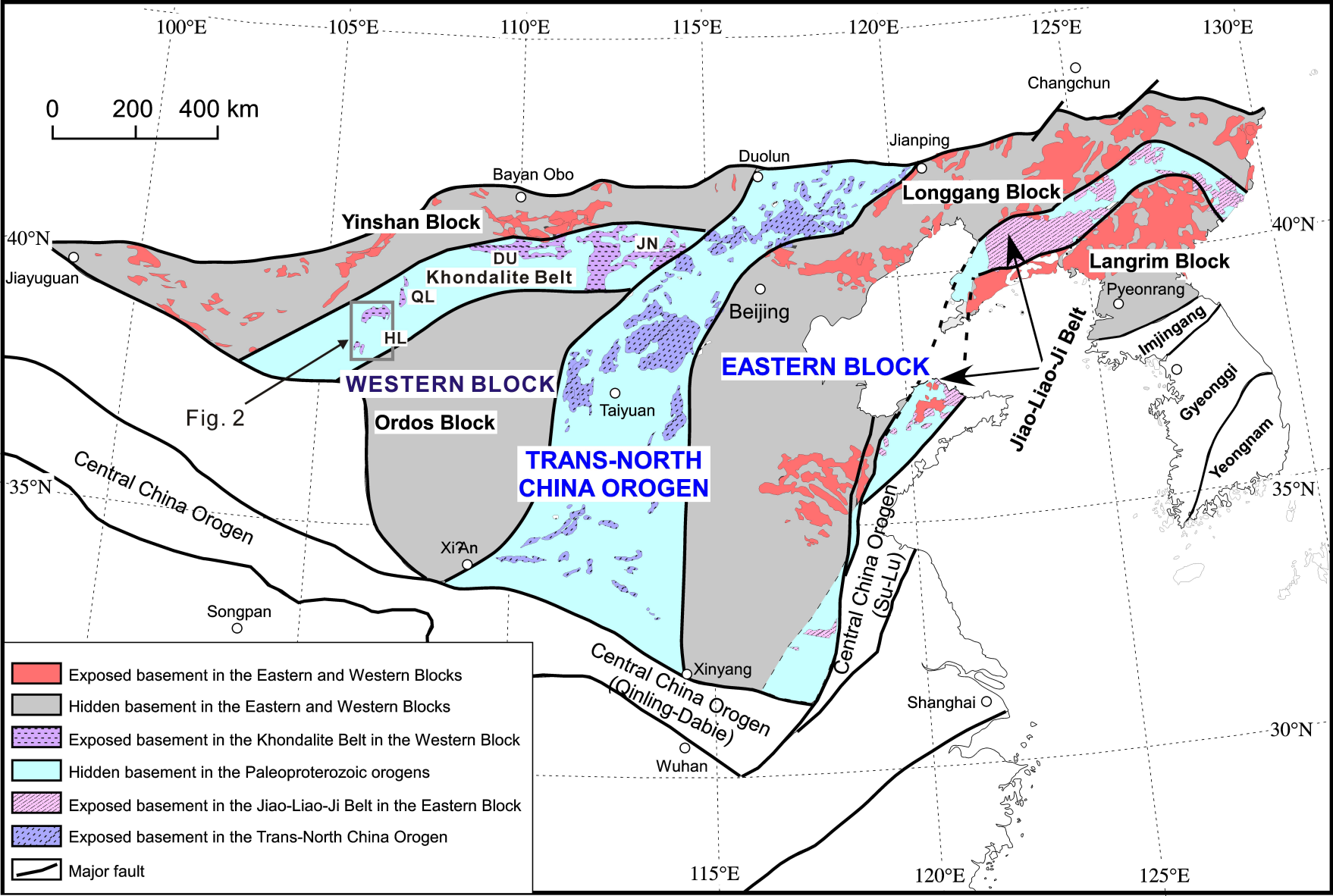
100°E
105°E
110°E
115°E
120°E
125°E
130°E
0 200 400 km
Changchun
Jianping
Duolun
Bayan Obo
Longgang Block
Yinshan Block
40°N
Jiayuguan
DU
JN
Khondalite Belt
QL
HL
Beijing
Langrim Block
Pyeonrang
Imjingang
Gyeonggi
Yeongnam
Jiao-Liao-Ji Belt
EASTERN BLOCK
WESTERN BLOCK
Fig. 2
Taiyuan
Ordos Block
TRANS-NORTH
CHINA OROGEN
35°N
Central China Orogen
Xi'An
Songpan
Central China Orogen
(Su-Lu)
Xinyang
Central China Orogen
(Qinling-Dabie)
Shanghai
Wuhan
30°N
115°E
120°E
125°E
Exposed basement in the Eastern and Western Blocks
Hidden basement in the Eastern and Western Blocks
Exposed basement in the Khondalite Belt in the Western Block
Hidden basement in the Paleoproterozoic orogens
Exposed basement in the Jiao-Liao-Ji Belt in the Eastern Block
Exposed basement in the Trans-North China Orogen
Major fault

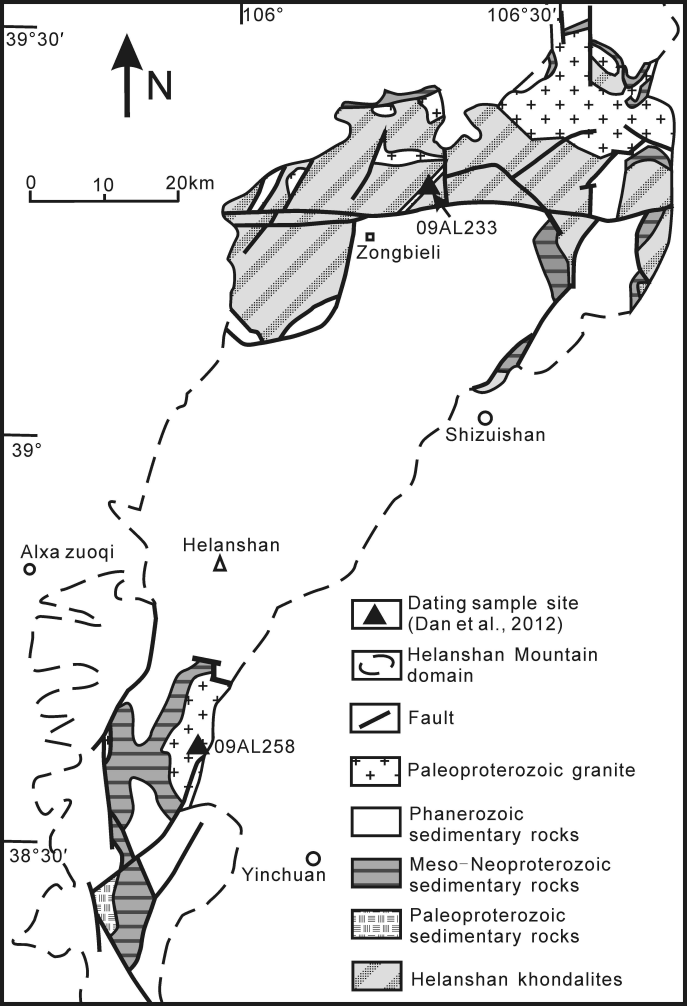
106°
106°30′
39°30′
N
0
10
20km
09AL233
Zongbieli
Shizuishan
39°
Alxa zuoqi
Helanshan
09AL258
38°30′
Yinchuan
Dating sample site (Dan et al., 2012)
Helanshan Mountain domain
Fault
Paleoproterozoic granite
Phanerozoic sedimentary rocks
Meso–Neoproterozoic sedimentary rocks
Paleoproterozoic sedimentary rocks
Helanshan khondalites

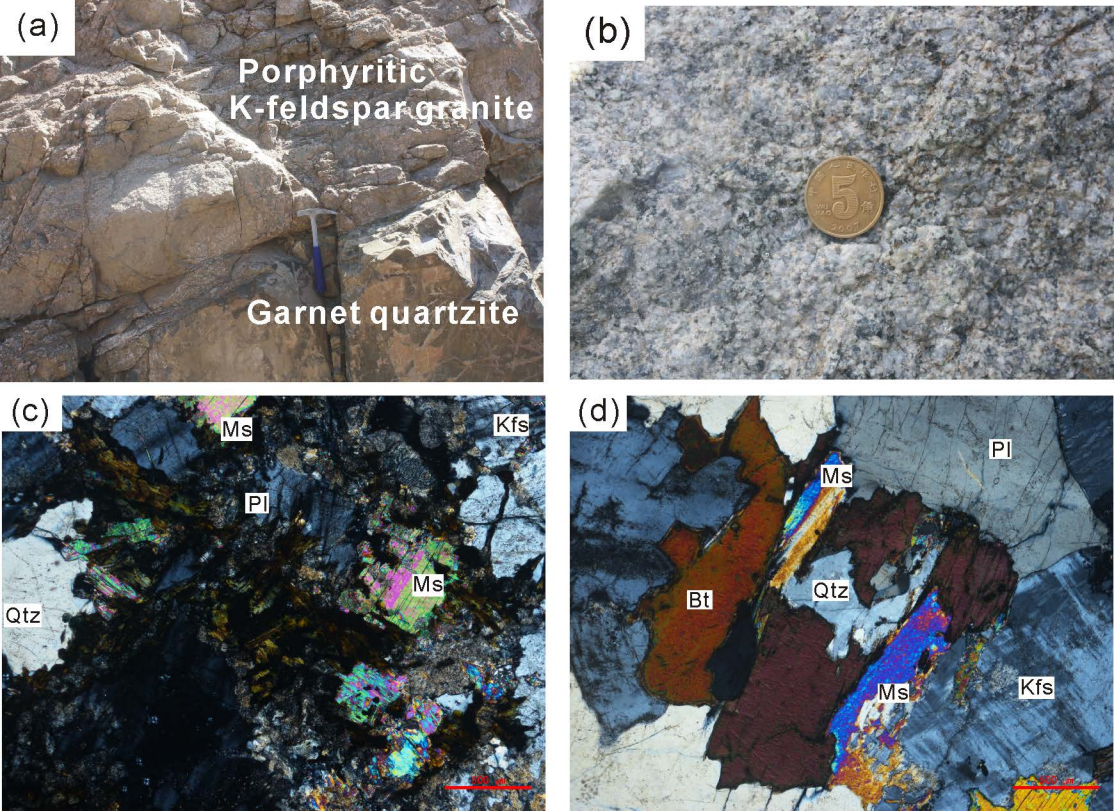
(a)
Porphyritic
K-feldspar granite
Garnet quartzite
(b)
(c)
Ms
Kfs
Pl
Ms
Qtz
(d)
Pl
Ms
Bt
Qtz
Ms
Kfs

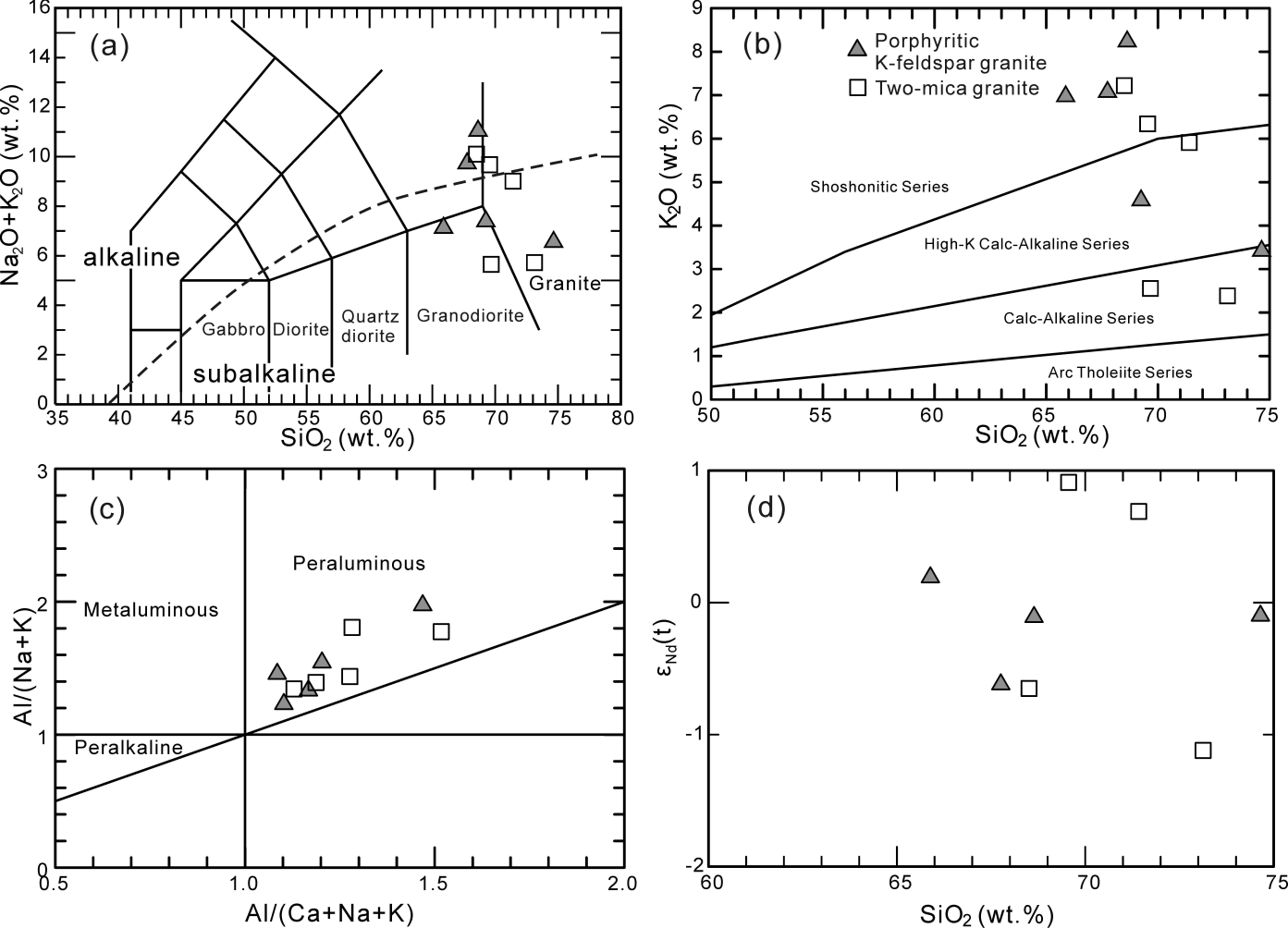
(a)
alkaline
subalkaline
Gabbro
Diorite
Quartz diorite
Granodiorite
Granite
Na2O+K2O (wt.%)
SiO2 (wt.%)
(b)
Porphyritic K-feldspar granite
Two-mica granite
Shoshonitic Series
High-K Calc-Alkaline Series
Calc-Alkaline Series
Arc Tholeiite Series
K2O (wt.%)
SiO2 (wt.%)
(c)
Peraluminous
Metaluminous
Peralkaline
Al/(Na+K)
Al/(Ca+Na+K)
(d)
εNd(t)
SiO2 (wt.%)

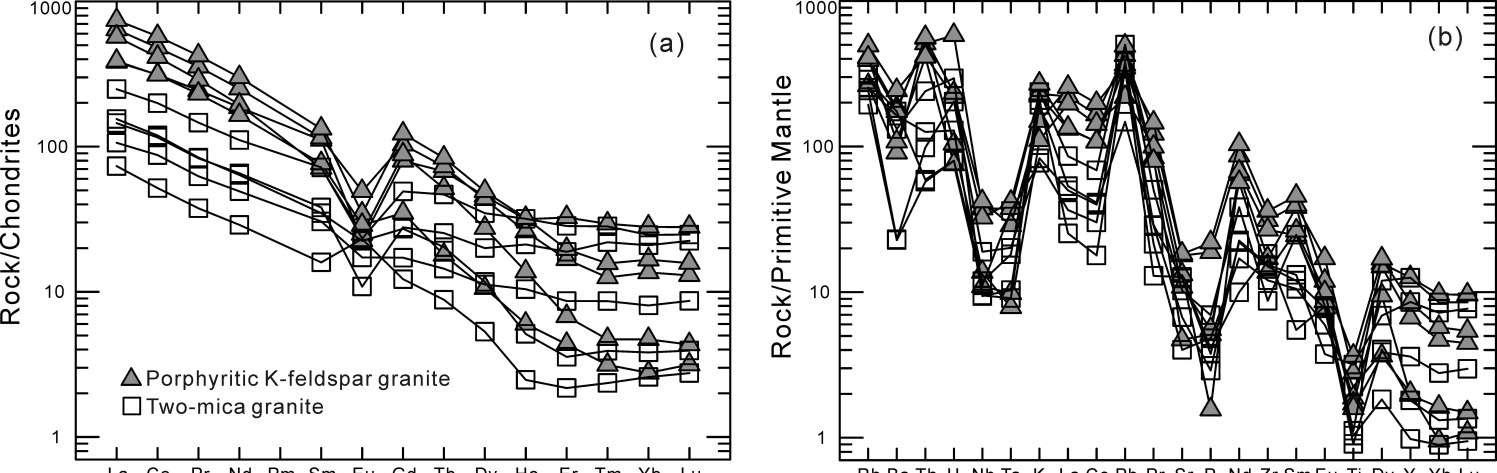
(a)
Rock/Chondrites
1000
100
10
1
La Ce Pr Nd Pm Sm Eu Gd Tb Dy Ho Er Tm Yb Lu
Porphyritic K-feldspar granite
Two-mica granite
(b)
Rock/Primitive Mantle
1000
100
10
1
Rb Ba Th U Nb Ta K La Ce Pb Pr Sr P Nd Zr Sm Eu Ti Dy Y Yb Lu

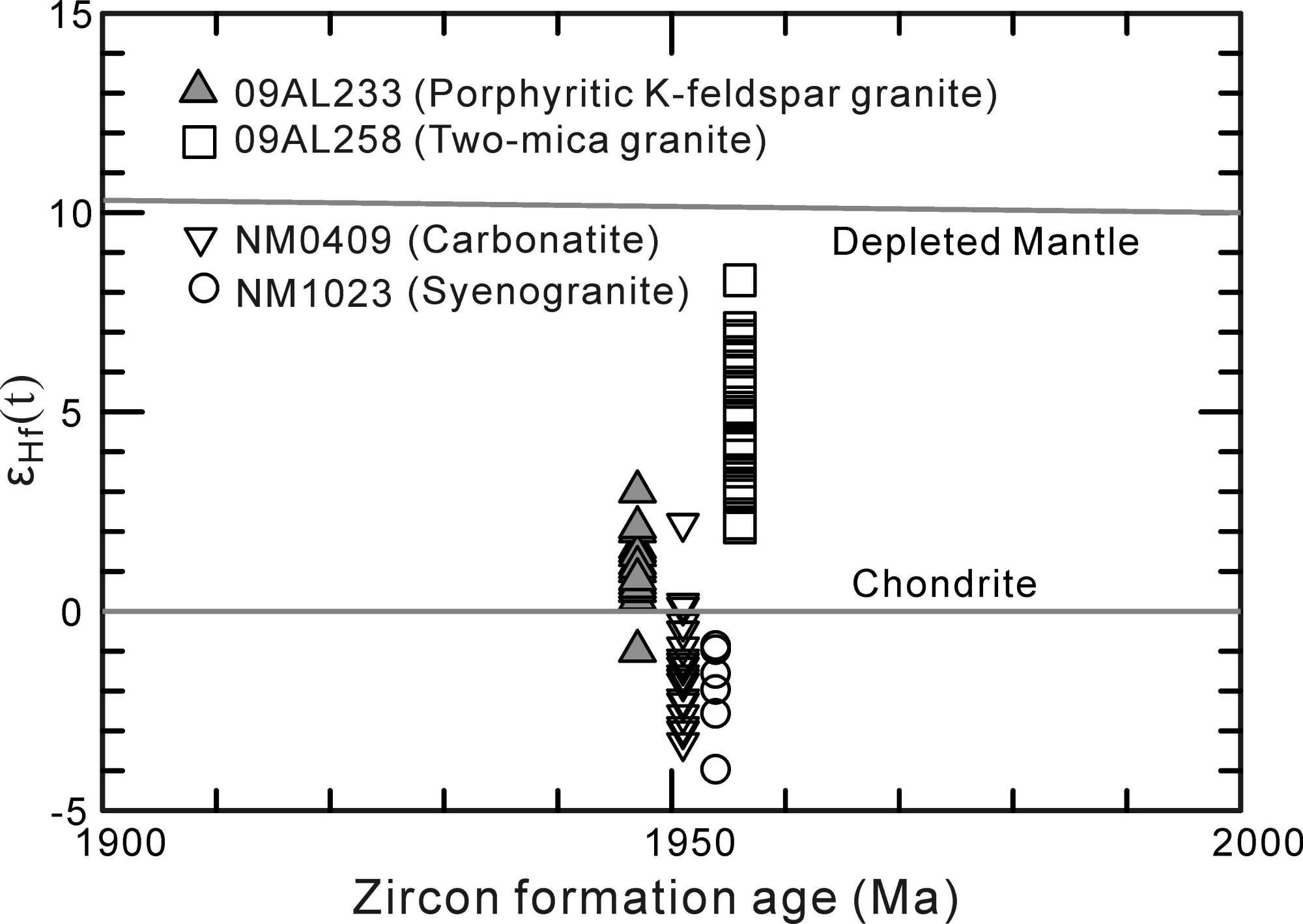
09AL233 (Porphyritic K-feldspar granite)
09AL258 (Two-mica granite)
NM0409 (Carbonatite)
NM1023 (Syenogranite)
Depleted Mantle
Chondrite
$\varepsilon_{Hf}(t)$
15
10
5
0
-5
1900
1950
2000
Zircon formation age (Ma)

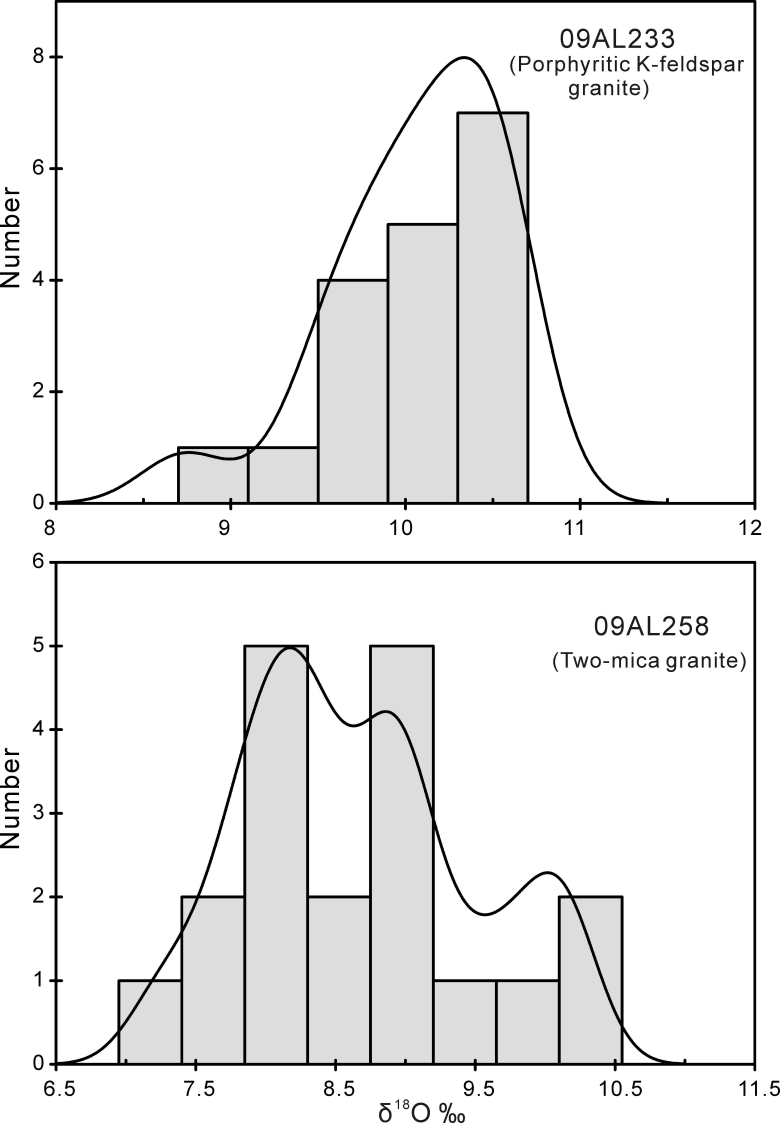
09AL233
(Porphyritic K-feldspar granite)
Number
0
2
4
6
8
8
9
10
11
12
09AL258
(Two-mica granite)
Number
0
1
2
3
4
5
6
6.5
7.5
8.5
9.5
10.5
11.5
δ18O ‰

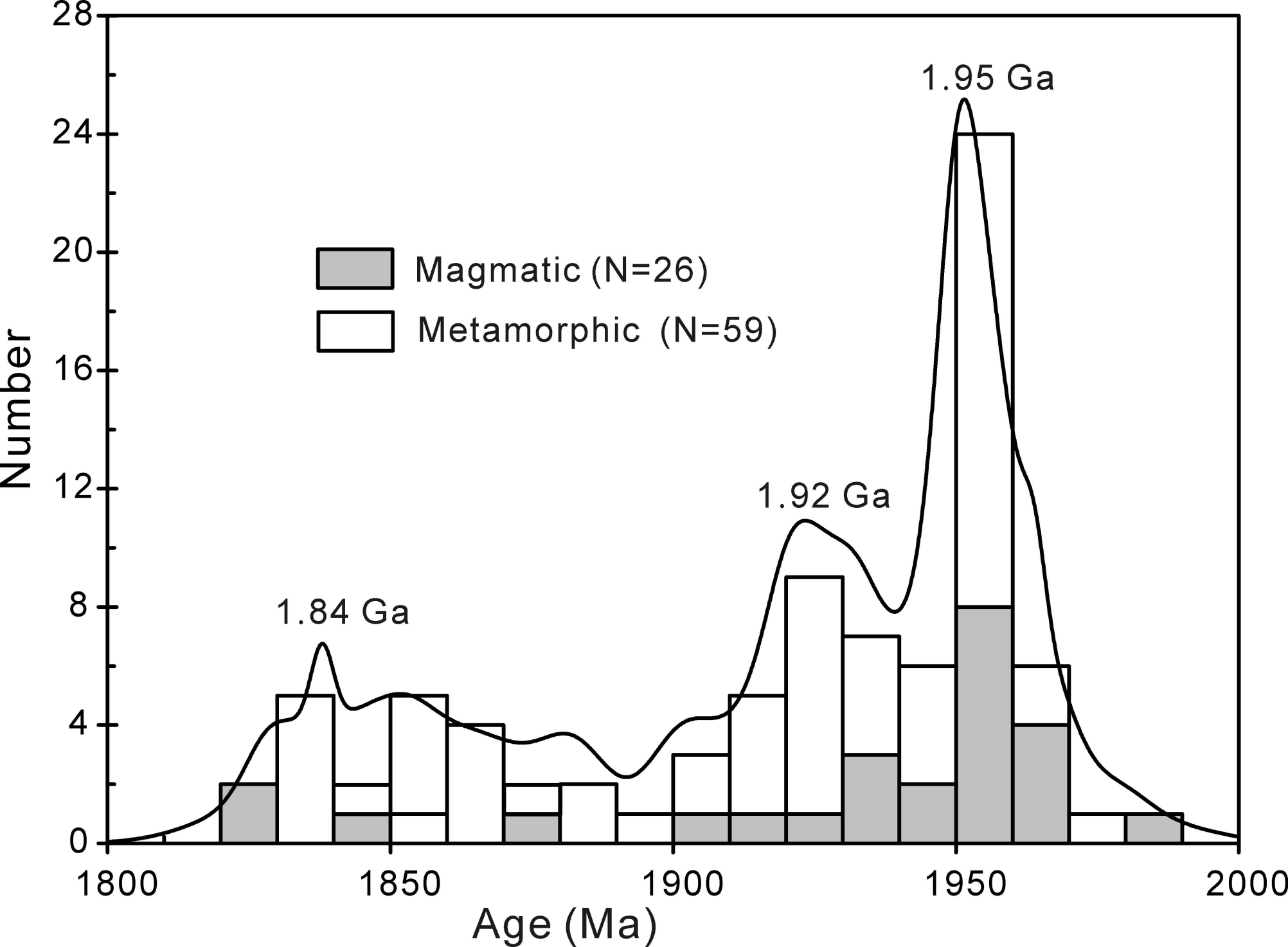
Magmatic (N=26)
Metamorphic (N=59)
1.95 Ga
1.92 Ga
1.84 Ga
Number
Age (Ma)
0
4
8
12
16
20
24
28
1800
1850
1900
1950
2000

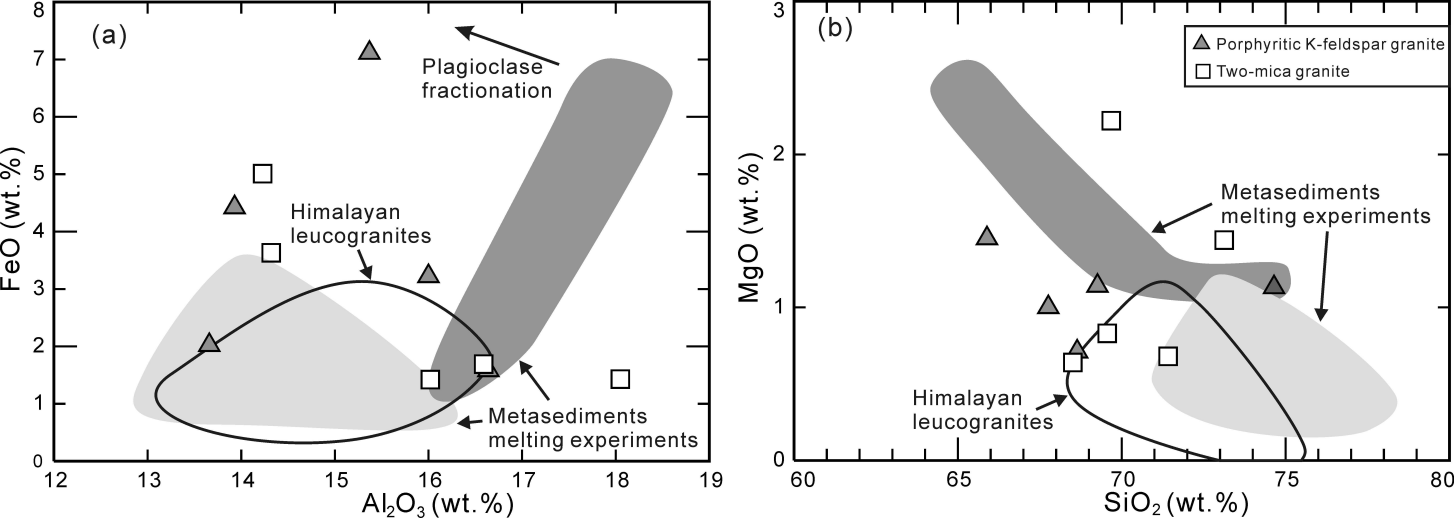
(a)
Plagioclase fractionation
Himalayan leucogranites
Metasediments melting experiments
FeO (wt.%)
Al2O3 (wt.%)
0
1
2
3
4
5
6
7
8
12
13
14
15
16
17
18
19
(b)
Porphyritic K-feldspar granite
Two-mica granite
Metasediments melting experiments
Himalayan leucogranites
MgO (wt.%)
SiO2 (wt.%)
0
1
2
3
60
65
70
75
80

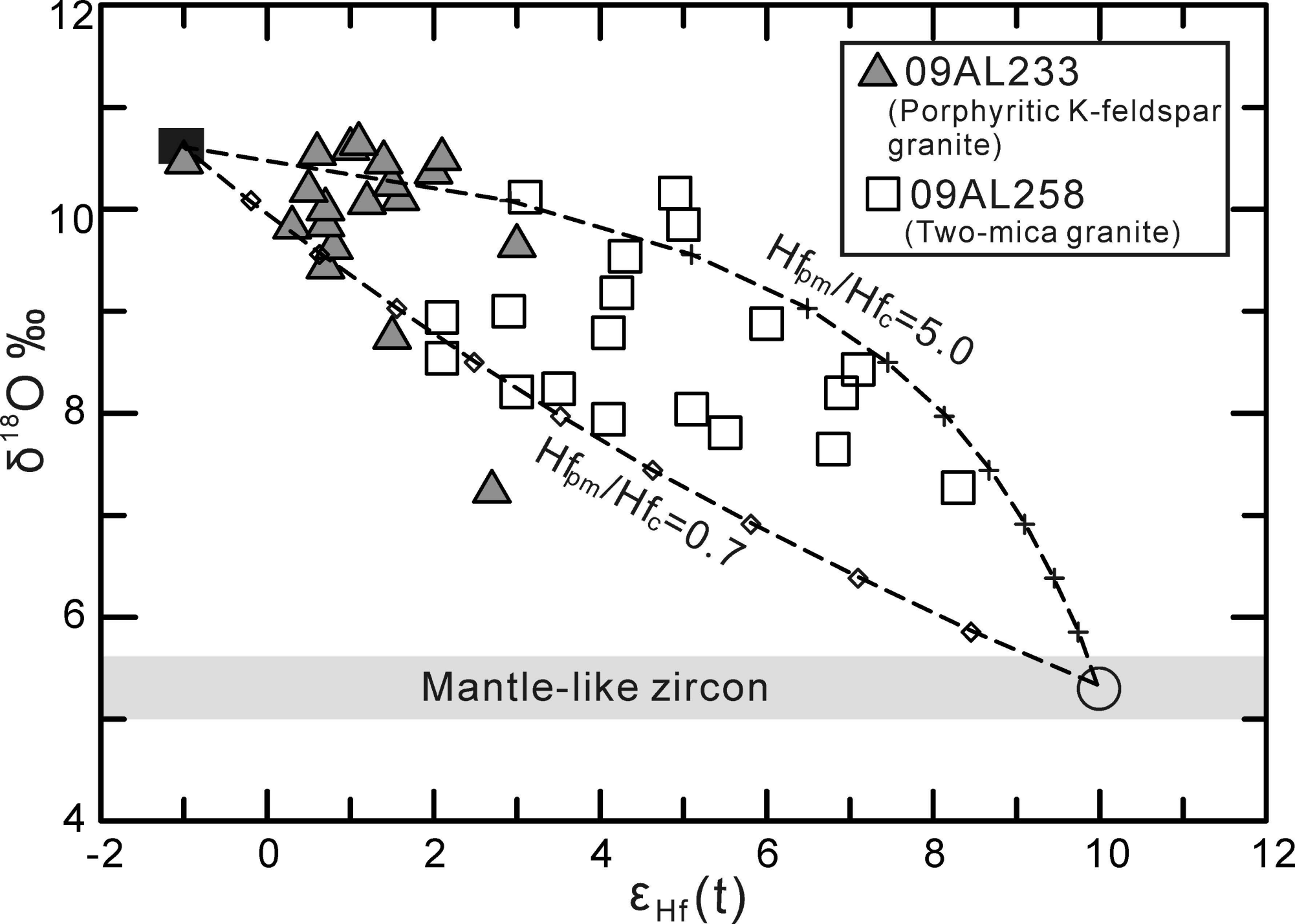
09AL233
(Porphyritic K-feldspar granite)
09AL258
(Two-mica granite)
Hfpm/Hfc=5.0
Hfpm/Hfc=0.7
Mantle-like zircon
δ18O ‰
εHf(t)
12
10
8
6
4
-2
0
2
4
6
8
10
12

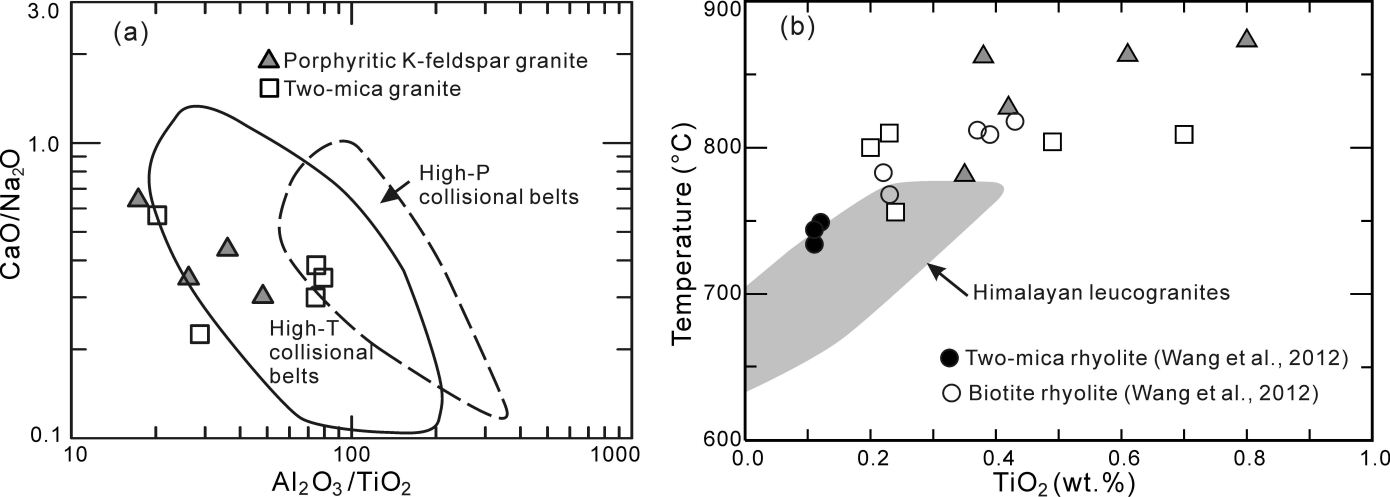
(a)
Porphyritic K-feldspar granite
Two-mica granite
High-P
collisional belts
High-T
collisional
belts
CaO/Na2O
Al2O3/TiO2
3.0
1.0
0.1
10
100
1000
(b)
Himalayan leucogranites
Two-mica rhyolite (Wang et al., 2012)
Biotite rhyolite (Wang et al., 2012)
Temperature (°C)
TiO2 (wt.%)
900
800
700
600
0.0
0.2
0.4
0.6
0.8
1.0

Table 1 Geochemical data for the ca. 1.95 Ga granites, Helanshan Complex

Sample	09AL225	09AL227	09AL228	09AL232	09AL233	09AL258	09AL259	09AL260	09AL261	09AL262
Rock type	Porphyritic K-feldspar granite					Two-mica granite				
Latitude(N)	39°17’01”	39°17’22”		39°18’17”		38°36’34”				
Longitude(E)	106°16’ 25”	106°17’03”		106°17’33”		105°56’05”				
Major element (%)										
SiO_2	65.89	67.76	69.26	74.65	68.64	71.42	69.56	68.51	69.68	73.13
TiO_2	0.42	0.61	0.80	0.38	0.35	0.20	0.23	0.24	0.70	0.49
Al_2O_3	15.37	16.00	13.93	13.66	16.64	16.02	16.59	18.05	14.23	14.32
$Fe_2O_3^T$	7.89	3.57	4.90	2.24	1.76	1.58	1.87	1.59	5.57	4.03
MnO	0.03	0.02	0.03	0.03	0.01	0.01	0.01	0.01	0.04	0.03
MgO	1.45	1.00	1.14	1.13	0.71	0.68	0.83	0.64	2.22	1.44
CaO	1.47	0.93	1.80	1.37	0.85	1.10	1.29	0.87	1.77	0.75
Na_2O	0.17	2.67	2.82	3.15	2.83	3.12	3.35	2.90	3.11	3.35
K_2O	6.95	7.05	4.56	3.40	8.21	5.89	6.32	7.20	2.54	2.37
P_2O_5	0.12	0.42	0.48	0.03	0.12	0.08	0.09	0.15	0.06	0.11
Total	99.74	100.03	99.73	100.04	100.13	100.09	100.13	100.16	99.92	100.01
L.O.I.	3.30	1.75	1.54	2.27	1.38	0.96	0.78	1.03	1.77	1.65
C	5.2	3.3	2.3	2.4	1.8	2.7	2.1	4.3	3.3	5.2
Mg#	28.8	38.1	33.9	52.7	47.1	48.5	49.4	46.9	46.7	44.1
A/CNK	1.47	1.17	1.08	1.20	1.10	1.18	1.13	1.27	1.28	1.52
T(°C)	825	860	870	860	778	798	807	754	807	803
Trace element (ppm)										
Sc	5.23	7.19	10.1	3.54	3.00	4.76	6.09	4.52	19.3	10.5
V	18.6	27.9	38.9	20.6	16.3	17.1	17.6	33.7	91.6	72.6
Cr	5.66	8.23	8.23	15.9	8.07	7.76	11.5	28.6	210	106
Co	6.22	4.66	7.37	3.49	3.22	2.95	3.59	4.14	12.6	10.0
Ni	5.02	4.39	4.92	7.80	3.85	5.15	7.19	9.08	37.1	17.4

Ga	22.7	22.7	23.1	18.1	18.8	14.4	15.5	15.7	19.6	16.2
Rb	262	313	248	167	258	161	183	197	154	123
Sr	99.4	376	386	279	229	262	268	216	142	84.7
Y	57.3	30.3	38.6	8.90	9.19	8.21	4.46	57.1	38.9	16.4
Zr	191	349	404	300	154	168	205	97.6	172	135
Nb	26.7	23.1	29.9	9.78	7.80	6.69	8.47	6.76	13.5	7.93
Cs	2.07	4.21	5.18	1.73	1.45	2.80	4.26	3.88	7.29	5.27
Ba	1283	1699	1221	634	754	1139	1215	921	161	159
La	90.7	152	176	135	92.0	36.7	17.4	59.0	34.4	25.2
Ce	192	294	352	253	191	73.1	31.7	122	70.9	53.5
Pr	23.2	33.7	40.2	27.4	21.9	7.98	3.57	13.9	7.88	5.93
Nd	87.1	117	140	90.8	76.8	29.8	13.5	51.8	30.6	23.0
Sm	17.0	17.6	20.3	10.9	11.7	5.32	2.44	11.0	5.83	4.67
Eu	1.31	2.86	2.00	1.45	1.67	1.30	1.34	1.35	0.63	1.00
Gd	16.4	21.2	25.2	18.1	7.18	5.59	2.51	10.1	5.71	3.53
Tb	2.53	2.73	3.13	1.93	0.67	0.76	0.33	1.75	0.95	0.54
Dy	11.6	11.0	12.5	6.97	2.69	2.97	1.35	8.83	5.08	2.85
Ho	1.79	1.47	1.82	0.78	0.34	0.29	0.14	1.80	1.20	0.59
Er	5.38	2.77	3.25	1.12	0.72	0.59	0.36	4.70	3.12	1.43
Tm	0.75	0.32	0.40	0.12	0.08	0.10	0.06	0.72	0.56	0.22
Yb	4.76	2.31	2.83	0.80	0.47	0.65	0.44	4.19	3.56	1.37
Lu	0.71	0.33	0.40	0.11	0.08	0.10	0.07	0.63	0.57	0.22
Hf	5.56	8.86	10.4	8.15	4.28	4.44	5.04	2.94	4.60	3.65
Ta	1.53	1.69	1.17	0.32	0.40	0.42	0.74	0.37	0.82	1.47
Pb	25.9	30.1	24.7	15.5	34.9	27.0	24.3	35.6	10.5	27.1
Th	43.3	35.8	47.3	47.8	35.1	10.7	5.03	20.4	8.37	4.87
U	12.2	4.58	4.90	2.19	1.58	2.71	1.68	6.18	4.27	1.68

Mg# = 100 × molar $Mg^{2+}/(Mg^{2+} + Fe^{2+})$, assuming $FeO/(FeO + Fe_2O_3) = 0.9$; A/CNK = molar $Al_2O_3/(CaO + Na_2O + K_2O)$; T(°C), zircon saturation temperature, calculated based on Watson and Harrison (1983). C = normative corundum.

Table 2 Whole rock Nd data for the ca. 1.95 Ga granites, Helanshan Complex

Sample	Sm	Nd	$^{147}Sm/^{144}Nd$	$^{143}Nd/^{144}Nd$	±2σ	$\varepsilon_{Nd}(t)$	T_{DM} (Ma)	T_{2DM} (Ma)
Porphyritic K-feldspar granite								
09AL225	17.0	87.1	0.1181	0.511640	0.000007	0.19	2404	2404
09AL227	17.6	117	0.0909	0.511249	0.000006	-0.62	2355	2470
09AL232	10.9	90.8	0.0725	0.511039	0.000006	-0.10	2274	2428
09AL233	11.7	76.8	0.0919	0.511287	0.000008	-0.11	2326	2429
Two-mica granite								
09AL258	5.32	29.8	0.1078	0.511532	0.000006	0.69	2324	2364
09AL259	2.44	13.5	0.1088	0.511557	0.000008	0.91	2312	2346
09AL260	11.0	51.8	0.1284	0.511728	0.000005	-0.65	2536	2472
09AL262	4.67	23.0	0.1225	0.511629	0.000007	-1.12	2538	2510

$\varepsilon_{Nd}(t)=10000\times\{[(^{143}Nd/^{144}Nd)_s-(^{147}Sm/^{144}Nd)_s\times(e^{\lambda t}-1)]/[(^{143}Nd/^{144}Nd)_{CHUR,0}-(^{147}Sm/^{144}Nd)_{CHUR}\times(e^{\lambda t}-1)]-1\}$;

$T_{DM}=1/\lambda\times\ln\{1+[(^{143}Nd/^{144}Nd)_s-(^{143}Nd/^{144}Nd)_{DM}]/[(^{147}Sm/^{144}Nd)_s-(^{147}Sm/^{144}Nd)_{DM}]\}$;

$T_{2DM}=T_{DM}-(T_{DM}-t)((f_c-f_s)/(f_c-f_{DM}))$; $f_{Sm/Nd}=(^{147}Sm/^{144}Nd)_s/(^{147}Sm/^{144}Nd)_{CHUR}-1$;

where f_c, f_s and f_{DM} are the $f_{Sm/Nd}$ values of the continental crust, sample and the depleted mantle; f_c = -0.4、f_{DM} = 0.08592; t = crystallization time; $(^{147}Sm/^{144}Nd)_s$ and $(^{143}Nd/^{144}Nd)_s$ are values of analysed sample; $(^{147}Sm/^{144}Nd)_{CHUR}$ = 0.1967 and $(^{143}Nd/^{144}Nd)_{CHUR,0}$ = 0.512638; $(^{147}Sm/^{144}Nd)_{DM}$ = 0.2135 and $(^{143}Nd/^{144}Nd)_{DM}$ = 0.51315; $(^{147}Sm/^{144}Nd)_c$ = 0.118; λ_{Sm-Nd} = 0.00654 Ga^{-1}.

Table 3 *In situ* zircon Hf-O isotopic results for the ca. 1.95 Ga granites in Helanshan Complex

Sample Spot	Age (Ma)	$^{176}Lu/^{177}Hf$	$^{176}Hf/^{177}Hf$	2σ	$\varepsilon_{Hf}(t)$	2σ	T_{DM} (Ma)	T_{DM}^{C} (Ma)	$\delta^{18}O$ (‰)
09AL233									
09AL233@1	1947	0.000766	0.281658	0.000035	3.0	1.2	2222	2405	9.64
09AL233@2	1947	0.000891	0.281619	0.000032	1.5	1.1	2282	2502	10.24
09AL233@3	1947	0.000855	0.281590	0.000025	0.5	0.9	2320	2567	10.18
09AL233@4	1947	0.000747	0.281606	0.000022	1.2	0.8	2292	2521	10.06
09AL233@5	1947	0.000916	0.281586	0.000022	0.3	0.8	2329	2579	9.82
09AL233@6	1947	0.001152	0.281558	0.000026	-1.0	0.9	2381	2662	10.46
09AL233@7	2058	0.000789	0.281581	0.000028	2.7	1.0	2328	2508	7.23
09AL233@8	1947	0.000843	0.281594	0.000027	0.7	1.0	2313	2555	9.43
09AL233@9	1947	0.000874	0.281595	0.000024	0.7	0.9	2314	2555	9.84
09AL233@10	1947	0.001003	0.281613	0.000024	1.1	0.8	2297	2526	10.64
09AL233@11	1947	0.001679	0.281625	0.000024	0.7	0.8	2321	2555	10.00
09AL233@12	1947	0.000909	0.281599	0.000024	0.8	0.8	2310	2549	9.62
09AL233@13	1947	0.001317	0.281650	0.000023	2.0	0.8	2266	2470	10.36
09AL233@14	1947	0.000834	0.281618	0.000021	1.5	0.7	2280	2500	8.74
09AL233@15	1947	0.000892	0.281605	0.000021	1.0	0.7	2301	2535	10.59
09AL233@16	1947	0.000871	0.281620	0.000023	1.6	0.8	2279	2498	10.10
09AL233@17	1947	0.000875	0.281593	0.000022	0.6	0.8	2317	2562	10.54
09AL233@18	1947	0.000606	0.281626	0.000017	2.1	0.6	2256	2464	10.49
09AL233@19	1947	0.000915	0.281619	0.000025	1.4	0.9	2284	2506	10.46
09AL233@20	1947	0.000890	0.281595	0.000022	0.6	0.8	2315	2557	n.d.

09AL233@21	1947	0.000920	0.281602	0.000020	0.8	0.7	2307	2544	n.d.
09AL258									
09AL258@1	1956	0.001768	0.281704	0.000026	3.5	0.9	2217	2379	8.24
09AL258@2	1956	0.001665	0.281743	0.000017	5.1	0.6	2155	2280	8.04
09AL258@3	1956	0.002140	0.281700	0.000018	2.9	0.6	2245	2419	9.00
09AL258@4	1956	0.002339	0.281821	0.000017	6.9	0.6	2084	2161	8.20
09AL258@5	1956	0.001078	0.281720	0.000014	5.0	0.5	2155	2285	9.85
09AL258@6	1956	0.001575	0.281735	0.000029	4.9	1.0	2162	2292	10.16
09AL258@7	1956	0.001115	0.281639	0.000028	2.1	1.0	2269	2472	8.54
09AL258@8	1956	0.001515	0.281713	0.000027	4.2	1.0	2189	2336	9.18
09AL258@9	1956	0.001449	0.281714	0.000022	4.3	0.8	2184	2328	9.54
09AL258@10	1956	0.003042	0.281884	0.000029	8.3	1.0	2033	2076	7.27
09AL258@11	1956	0.002117	0.281817	0.000021	7.1	0.7	2077	2150	8.43
09AL258@12	1956	0.002791	0.281727	0.000021	3.0	0.7	2245	2412	8.21
09AL258@13	1956	0.001350	0.281649	0.000021	2.1	0.7	2269	2469	8.94
09AL258@14	1956	0.002042	0.281701	0.000029	3.1	1.0	2237	2408	10.12
09AL258@15	1956	0.002179	0.281811	0.000021	6.8	0.8	2089	2169	7.65
09AL258@16	1956	0.001718	0.281770	0.000025	6.0	0.9	2121	2224	8.88
09AL258@17	1956	0.002361	0.281743	0.000019	4.1	0.7	2197	2340	8.79
09AL258@18	1956	0.001507	0.281709	0.000021	4.1	0.7	2194	2345	7.94
09AL258@19	1956	0.002090	0.281772	0.000026	5.5	0.9	2139	2251	7.81
09AL258@20	1956	0.001504	0.281705	0.000021	3.9	0.7	2199	2353	n.d.
09AL258@21	1956	0.001330	0.281678	0.000028	3.2	1.0	2226	2400	n.d.
09AL258@22	1956	0.001607	0.281781	0.000024	6.5	0.9	2099	2190	n.d.
09AL258@23	1956	0.001129	0.281765	0.000024	6.5	0.9	2095	2186	n.d.

09AL258@24	1956	0.002408	0.281808	0.000031	6.4	1.1	2107	2196	n.d.
09AL258@25	1956	0.000919	0.281772	0.000035	7.1	1.2	2073	2151	n.d.
09AL258@26	1956	0.001955	0.281769	0.000017	5.6	0.6	2136	2246	n.d.
09AL258@27	1956	0.001793	0.281667	0.000022	2.2	0.8	2270	2465	n.d.
09AL258@28	1956	0.001365	0.281759	0.000018	6.0	0.6	2117	2220	n.d.

n.d. = not determined.

$\varepsilon_{Hf(t)} = 10000\{[(^{176}Hf/^{177}Hf)_s - (^{176}Lu/^{177}Hf)_s \times (e^{\lambda t} - 1)]/[(^{176}Hf/^{177}Hf)_{CHUR(0)} - (^{176}Lu/^{177}Hf)_{CHUR} \times (e^{\lambda t} - 1)] - 1$; $T_{DM} = 1/\lambda \times \ln\{1 + [(^{176}Hf/^{177}Hf)_s - (^{176}Hf/^{177}Hf)_{DM}]/[(^{176}Lu/^{177}Hf)_s - (^{176}Lu/^{177}Hf)_{DM}]\}$; $T_{DM}^{C} = T_{DM} - (T_{DM} - t) \times [f_{cc} - f_s/(f_{cc} - f_{DM})]$; $f_{Lu/Hf} = (^{176}Lu/^{177}Hf)_s/(^{176}Lu/^{177}Hf)_{CHUR} - 1$; where, f_{CC}, f_S and f_{DM} are the $f_{Lu/Hf}$ values of the continental crust, zircon sample and the depleted mantle; subscript S = analyzed zircon sample, CHUR = chondritic uniform reservoir; DM = depleted mantle; t = crystallization time or metamorphic time of zircon; $\lambda = 1.867\times10^{-11}$ year^{-1}; $^{176}Hf/^{177}Hf_{DM} = 0.28325$; $^{176}Lu/^{177}Hf_{DM} = 0.0384$; present-day $^{176}Hf/^{177}Hf_{CHUR(0)} = 0.282772$; $^{176}Lu/^{177}Hf_{CHUR} = 0.0332$; $^{176}Hf/^{177}Hf_{CC} = 0.015$.